Biogeosciences Open Access
Discussions
EGU

1 **Long chain diols in settling particles in tropical oceans:**

2 **insights into sources, seasonality and proxies.**

3

4 Marijke W. de Bar[*,1], Jenny E. Ullgren[2], Robert C. Thunnell[‡], Stuart G. Wakeham[3], Geert-Jan

5 A. Brummer[4,5], Jan-Berend W. Stuut[4,5], Jaap S. Sinninghe Damsté[1,6] and Stefan Schouten[1,6]

6

7 [1] NIOZ Royal Netherlands Institute for Sea Research, Department of Marine Microbiology

8   and Biogeochemistry, and Utrecht University, P.O. Box 59, 1790 AB Den Burg, Texel, the

9   Netherlands

10 [2] Runde Miljøsenter, Runde, Norway

11 [3] Skidaway Institute of Oceanography, University of Georgia, 10 Ocean Science Circle,

12   Savannah, USA

13 [4] NIOZ Royal Netherlands Institute for Sea Research, Department of Ocean Systems, and

14   Utrecht University, P.O. Box 59, 1790 AB Den Burg, Texel, the Netherlands

15 [5] Vrije Universiteit Amsterdam, Faculty of Science, Department of Earth Sciences, De

16   Boelelaan 1085, 1081HV Amsterdam, the Netherlands

17 [6] Department of Earth Sciences, Faculty of Geosciences, Utrecht University, the Netherlands

18

19 * Corresponding author: Marijke W. de Bar (Marijke.de.Bar@nioz.nl)

20

21

[‡] Deceased: 30 July 2018.

Biogeosciences Open Access
Discussions
EGU

22   **ABSTRACT**

23   In this study we have analyzed sediment trap time series from five tropical sites to assess seasonal

24   variations in concentrations and fluxes of long-chain diols (LCDs) and associated proxies with emphasis

25   on the Long chain Diol Index (LDI). For the tropical Atlantic, we observe that generally less than 2 %

26   of LCDs settling from the water column are preserved in the sediment. The Atlantic and Mozambique

27   Channel traps reveal minimal seasonal variations in the LDI, similar to the TEX_{86} and $U^{K'}_{37}$. However,

28   annual mean LDI-derived temperatures are in good agreement with the annual mean satellite-derived

29   sea surface temperatures (SSTs). In the Cariaco Basin the LDI shows larger seasonal variation, as do

30   the TEX_{86} and $U^{K'}_{37}$. Here, the LDI underestimates SST during the warmest months, which is likely due

31   to summer stratification and the habitat depth of the diol producers deepening to around 20 to 30 m.

32   Surface sediment LDI temperatures in the Atlantic and Mozambique Channel compare well with the

33   average LDI-derived temperatures from the overlying sediment traps, as well as with decadal annual

34   mean SST. Lastly, we observed large seasonal variations in the Diol Index, as indicator of upwelling

35   conditions, at three sites, potentially linked to Guinea Dome upwelling (Eastern Atlantic), seasonal

36   upwelling (Cariaco Basin) and seasonal upwelling and/or eddy migration (Mozambique Channel).

37

1. Introduction

Several proxies exist for the reconstruction of past sea surface temperature (SST) based on lipids. The $U^{K'}_{37}$ is one of the most applied proxies and is based on the unsaturation of long-chain alkenones (LCAs), which are produced by phototrophic haptophyte algae, mainly the cosmopolitan *Emiliania huxleyi* (Volkman et al., 1980; Brassell et al., 1986; Prahl and Wakeham, 1987; Conte et al., 1994). This index exhibits a strong positive correlation with SST (Müller et al., 1998; Conte, 2006). Another widely used organic paleotemperature proxy is the TEX_{86}, as originally proposed by Schouten et al. (2002), based on the relative distribution of archaeal membrane lipids, i.e. glycerol dialkyl glycerol tetraethers (GDGTs), and in the marine realm are mainly thought to be derived from the phylum Thaumarchaeota. Schouten et al. (2002) showed that the TEX_{86} index measured in marine surface sediments is correlated with SST, and since then its application in paleoenvironmental studies has increased. However, research showed that despite the highest abundance of Thaumarchaeota in the upper 100 m of the water column, they can be present down to 5000 m depth (Karner et al., 2001; Herndl et al., 2005). Accordingly, GDGTs may be found in high concentrations below 100 m depth (e.g., Sinninghe Damsté et al., 2002; Wuchter et al., 2005) and several studies have indicated that TEX_{86} might be more reflective of subsurface temperatures in some regions (e.g., Huguet et al., 2007; Lopes dos Santos et al., 2010; Kim et al., 2012; 2015; Schouten et al., 2013; Chen et al., 2014; Tierney et al., 2017; see Zhang and Liu, 2018 for review).

Most recently a SST proxy based on the distribution of long-chain diols (LCDs), called the Long-chain Diol Index, or LDI was proposed (Rampen et al., 2012). This index is a ratio of 1,13- and 1,15-diols (i.e., alcohol groups at position C-1 and C-13 or C-15), and the analysis of globally distributed surface sediments revealed that this index strongly correlates with SST. Since then, the index has been applied in several paleoenvironmental studies (e.g., Naafs et al., 2012; Lopes dos Santos et al., 2013; Jonas et al., 2017; Warnock et al., 2017). However, large gaps still remain in the understanding of this proxy. The largest uncertainty is that the main marine producer of LCDs is unknown. Although these diols have been observed in cultures of certain marine eustigmatophyte algae (e.g. Volkman et al., 1992; 1999; Méjanelle et al., 2003; Rampen et al., 2014b), the LCD distributions in cultures are different from those

65   observed in marine sediments. Furthermore, Balzano et al. (2018) combined lipid analyses with 18S

66   rRNA gene amplicon sequencing on suspended particulate matter (SPM) and did not find a significant

67   direct correlation between LCD concentrations and sequences of known LCD-producers. Rampen et al.

68   (2012) observed the strongest empirical relation between surface sediment derived LDI values and SSTs

69   for autumn to summer, suggesting that these are the main growth seasons of the source organisms.

70   Moreover, the strongest correlation was also observed for the upper 20 m of the water column,

71   suggesting that the LCDs are likely produced by phototrophic algae which thrive in the euphotic zone.

72   Nevertheless, LDI-temperatures based on surface sediments reflect an integrated signal of many years,

73   which complicates the interpretation of the LDI in terms of seasonal production and depth of export

74   production.

75   One way of resolving seasonality in LCD flux and LDI is to analyze time series samples from sediment

76   traps that continuously collect sinking particles in successive time intervals over periods of a year or

77   more. Such studies have been carried out for the $U^{K'}_{37}$ as well as for the TEX_{86} and associated lipids

78   (e.g., Müller and Fischer, 2001; Wuchter et al., 2006; Huguet et al., 2007; Fallet et al., 2011; Yamamoto

79   et al., 2012; Rosell-Melé and Prahl, 2013; Türich et al., 2013). However, very few studies have been

80   done for LCDs. Villanueva et al. (2014) carried out a sediment trap study in Lake Challa (East Africa)

81   and Rampen et al. (2008) in the upwelling region off Somalia. The latter study showed that 1,14-diols,

82   produced by *Proboscia* diatoms strongly increased early in the upwelling season in contrast to 1,13- and

83   1,15-diols and thus can be used to trace upwelling. However, none of these sediment trap studies have

84   evaluated the LDI.

85   In this study, we assess seasonal patterns of the LDI for sediment trap series at five sites, i.e., in the

86   Cariaco Basin, the Mozambique Channel and three sites in the tropical North Atlantic and compared the

87   LDI values to satellite-derived SST, as well as results obtained for other temperature proxies, i.e. the

88   TEX^{H}_{86} and $U^{K'}_{37}$. Moreover, for the Atlantic and Mozambique Channel, we compare the sediment trap

89   proxy signals with those preserved in the underlying sediments, after settling and burial. Finally, we

90   assess the applicability of the Diol Index, based on 1,14-diols produced by *Proboscia* diatoms

91   (Sinninghe Damsté et al., 2003), as tracer of upwelling and/or productivity in these regions.

Biogeosciences
Discussions

Open Access

EGU

2. Materials and methods

2.1 Study sites and sample collection

2.1.1 Tropical North Atlantic

The ocean current and wind patterns of the tropical Atlantic are mostly determined by the seasonal

latitudinal shift of the intertropical convergence zone (ITCZ; Figure 1). The ITCZ migrates southward

during boreal winter, and northward during boreal summer. During summer, the south-east trade winds

prevail, whereas during winter the north-east trade winds intensify. The north-east trade winds drive the

North Equatorial Current (NEC) which flows westward. South of this current flows the North Equatorial

Countercurrent (NECC) towards the east (Stramma and Schott, 1999). The South Equatorial Current

flows westward and branches off in the north Brazil Current (NBC; Stramma and Schott, 1999). When

the ITCZ is in the north, the NBC retroflects off the South American coast, and is carried eastward into

the NECC, and thus into the western tropical Atlantic (e.g., Richardson and Reverdin, 1987). North of

the NBC, the Guiana Current (GC) disperses the outflow from the Amazon River towards the Caribbean

Sea. (Müller-Karger et al., 1988; 1995). However, during boreal summer the NBC may retroflect,

carrying the Amazon River plume far into the western Atlantic (e.g., Lefèvre et al., 1998; Müller-Karger

et al., 1998; Coles et al., 2013). In fact, every late summer/autumn, the Amazon River outflow covers

around 2×10^6 km^2 of the western North Atlantic, and the river delivers approximately half of all

freshwater input into the tropical Atlantic (see Araujo et al., 2017 and references therein).

The eastern tropical North Atlantic is characterized by upwelling caused by the interaction between the

trade winds and the movement of the ITCZ. Cropper et al. (2014) measured upwelling intensity along

the NW African coastline between 1981 and 2012, in terms of wind speed, SST and other meteorological

data. They recognized three latitudinal zones: weak permanent annual upwelling north of 26° N, strong

permanent upwelling between 21° and 26° N and seasonal upwelling between 12° and 19° N related to

the seasonal migration of the trade winds. Southeast of Cape Verde, large-scale cyclonic circulation

forms the Guinea Dome (GD; Fig. 1), which centers around 10° N/22° W (Mazeika, 1967), i.e., close to

mooring site M1. It is a thermal upwelling dome, formed by near-surface flow fields associated with the

westward NEC, eastward NECC and the westward North Equatorial Undercurrent (NEUC) (Siedler et

119   al., 1992). It forms a cyclonic circulation as result of the eastward flowing NECC and the westward

120   flowing NEC (Rossignol and Meyrueis, 1964; Mazeika, 1967). The GD develops from late spring to

121   late fall due to the northward ITCZ position and the resulting Ekman upwelling, but shows significant

122   interannual variability (Siedler et al., 1992; Yamagata and Iizuka, 1995; Doi et al., 2009) judging from

123   general ocean circulation models. According to Siedler et al. (1992), upwelling is most intense between

124   July and October when the ITCZ is in the GD region and the NECC is strongest.

125   At three sites, we analyzed five sediment trap series along a latitudinal transect in the North Atlantic

126   (~12° N) to determine seasonal variations in the LDI. This transect has been studied previously for

127   Saharan dust deposition in terms of grain sizes (van der Does et al., 2016), as the tropical North Atlantic

128   receives approximately one third of the wind-blown Saharan dust (e.g., Duce et al., 1991; Stuut et al.,

129   2005), which might potentially act as fertilizer because of the high iron levels (e.g., Martin and

130   Fitzwater, 1988; Korte et al., 2017; Guirreiro et al., 2017; Goudie and Middleton, 2001 and references

131   therein). Furthermore, Korte et al. (2017) assessed mass fluxes and mineralogical composition,

132   Guerreiro et al. (2017) measured coccolith fluxes for two of the time series, while Schreuder et al.

133   (2018a; 2018b) measured long chain *n*-alkanes, long chain *n*-alkanols and fatty acids, and levoglucosan

134   for the same sediment trap samples and surface sediments as analyzed in this study.

135   At site M1 (12.00° N, 23.00° W), the sediment trap, referred to as M1U, was moored at a water depth

136   of 1150 m (Fig. 1). This mooring is located in the proximity of the Guinea Dome, and might therefore

137   potentially be influenced by seasonal upwelling. At station M2 (13.81° N, 37.82° W), two sediment

138   traps were recovered, i.e., an 'upper' (M2U) trap at a water depth of 1235 m, and a 'lower' (M2L) trap

139   at a depth of 3490 m. Lastly, at mooring station M4 (12.06° N, 49.19° W), also an upper and lower trap

140   series were recovered and analyzed (M4U and M4L), at 1130 and 3370 m depth, respectively. This

141   mooring site may seasonally be affected by Amazon River discharge (van der Does et al., 2016; Korte

142   et al., 2017; Guirreiro et al., 2017; Schreuder et al., 2018a). All sediment traps were equipped with 24

143   sampling cups, which sampled synchronously over 16-day intervals from October 2012 to November

144   2013, using $HgCl_2$ as a biocide and borax as a pH buffer to prevent in situ decomposition of the collected

145   material.

146

2.1.2   Mozambique Channel

147

148   The Mozambique Channel is located between Madagascar and Mozambique and is part of the Agulhas

149   Current system hugging the coast of South Africa (Lutjeharms, 2006). The Agulhas Current system is

150   an important conveyor in the transport of warm and salty waters from the Indian to the Atlantic Ocean

151   (Gordon, 1986; Weijer et al., 1999; Peeters et al., 2004). The northern part of the channel is also

152   influenced by the East African monsoon winds (Biastoch and Krauss, 1999; Sætre and da Silva, 1982;

153   Malauene et al., 2014). Between September and March, these winds blow from the northeast, parallel

154   to the Mozambique coastline, favoring coastal upwelling. Additionally, the Mozambique Channel is

155   largely influenced by fast-rotating, mesoscale eddies which migrate southward towards the Agulhas

156   region. Using satellite altimetry, Schouten et al. (2003) observed on average 4 to 6 eddies, ca. 300 km

157   in diameter, propagating yearly from the central Mozambique Channel (15° S) toward the Agulhas area

158   (35° S) between 1995 and 2000. Seasonal upwelling occurs off Northern Mozambique (between ca. 15

159   and 18° S) (Nehring et al., 1987; Malauene et al., 2014), from August to March with a dominant period

160   of about two months although periods of one to four weeks have also been observed (Malauene et al.,

161   2014).

162   The sediment trap was moored at 16.8° S and 40.8° E, at a water depth of 2250 m (Fig. 1; Fallet et al.,

163   2010, 2011) and of the same type as used for the North Atlantic transect. We analyzed the LCD proxies

164   for two respective time intervals: the first interval covers ca. 3.5 years, from November 2003 to

165   September 2007, with a sampling interval of 21 days. The second interval covers another year, between

166   February 2008 and February 2009, with a sampling interval of 17 days. Previously, Fallet et al. (2011)

167   published foraminiferal, $U^{K'}_{37}$ and TEX_{86} records for the first time interval, and the organic carbon

168   content for the follow-up time series. For further details on the deployments and sample treatments, we

169   refer to Fallet et al. (2011, 2012). The two surface sediments are located across the narrowest transect

170   between Mozambique and Madagascar, and were analyzed for $U^{K'}_{37}$ and TEX_{86} by Fallet et al. (2012)

171   and for LCDs by Lattaud et al. (2017b).

172

2.1.3 Cariaco Basin

The Cariaco Basin is one of the largest marine anoxic basins (Richards, 1975), located on the continental

shelf of Venezuela. The basin is characterized by permanent stratification and strongly influenced by

the migration of the intertropical convergence zone (ITCZ). During late autumn and winter, the ITCZ

migrates to the south which results in decreased precipitation and trade wind intensification which in

turn induces upwelling and surface water cooling. This seasonal upwelling is a major source of nutrients

that leads to strong phytoplankton growth along the Venezuelan coast (e.g., Müller-Karger et al., 2001;

Thunell et al., 2007). Between August and October, the ITCZ moves northward again, resulting in a

rainy season and diminishing of the trade winds inhibiting upwelling. During this wet season the

contribution of terrestrially derived nutrients is higher. Due to the prevalent anoxic conditions in the

basin, there is no bioturbation which has resulted in the accumulation of varved sediments which provide

excellent annually to decadally resolved climate records (e.g., Peterson et al., 1991; Hughen et al., 1996;

1998). Moreover, in November 1995, a time series experiment started to facilitate research on the link

between biogeochemistry and the downward flux of particulate material under anoxic and upwelling

conditions (Thunell et al., 2000). This project (CARIACO; http://imars.marine.usf.edu/cariaco)

involved hydrographic cruises (monthly), water column chemistry measurements and sediment trap

sampling (every 14 days). One mooring containing four automated sediment traps (Honjo and Doherty,

1988) was deployed at 10.50° N and 64.67° W, at a bottom depth of around 1400 m. These traps were

moored at 275 m depth, just above the oxic/anoxic interface (Trap A), 455 m (Trap B), 930 m (Trap C)

and 1255 m (Trap D). All traps contain a 13-cup carousel which collected sinking particles over 2 weeks,

and were serviced every half year. For further details on trap deployment and recovery, and sample

collection, storage and processing we refer to Thunell et al. (2000) and Goñi et al. (2004). In addition to

the sediment trap sampling, the primary productivity of the surface waters was measured every month

using ^{14}C incubations (Müller-Karger et al., 2001; 2004). For this study, we investigated two periods,

i.e., May 1999–May 2000 and July 2002–July 2003 for Traps A and B. These years include upwelling

and non-upwelling periods, as well as a disastrous flooding event in December 1999 (Turich et al.,

2013). Turich et al. (2013) identified the upwelling periods, linked to the migration of the ITCZ, as

indicated by decreasing SST in the CTD and satellite-based measurements (indicated by grey boxes in

201 figures 9 and 10), and shoaling of the average depths of primary production and increased primary

202 production. Moreover, Turich et al. (2013) evaluated the $U^{K'}_{37}$ and TEX_{86} proxies for the same two time

203 series for which we analyzed the LCD proxies.

204

205 **2.2 Instrumental data**

206 Satellite SST, precipitation and wind speed time series of the M1, M2 and M4 moorings in the Atlantic

207 derive from Guerreiro et al. (2017 and in revision) who retrieved these data from the Ocean Biology

208 Processing Group (OBPG, 2014) (Frouin et al., 2003), the Goddard Earth Sciences Data and Information

209 Services Center (2016) (Huffman et al., 2007; Xie and Arkin, 1997) and NASA Aquarius project (2015a;

210 2015b) (Lee et al., 2012) (see supplement of Guerreiro et al., 2017 for detailed references). The SST and

211 Chlorophyll *a* time series data for the Mozambique Channel were adapted from Fallet et al. (2011), who

212 retrieved these data from the Giovanni database (for details see Fallet et al., 2011). Surface sediment

213 proxy temperatures were compared to annual mean SST estimates derived from the World Ocean Atlas

214 (2013) (decadal averages from 1955 to 2012; Locarnini et al., 2013). Sea surface temperature data for

215 the Cariaco Basin were adopted from Turich et al. (2013) and combined with additional CTD

216 temperatures from the CARIACO time series data base for the depths of 2, 5, 10, 15 and 20 m

217 (http://www.imars.usf.edu/CAR/index.html.; CARIACO time series composite CTD profiles; lead

218 principal investigator: Frank Müller-Karger).

219

220 **2.3 Lipid extraction**

221 **2.3.1 Tropical North Atlantic**

222 The 120 sediment trap samples were sieved through a 1 mm mesh wet-split into five aliquots (van der

223 Does et al., 2016), of which one was washed with Milli-Q water, freeze-dried and homogenized for

224 chemical analysis (Korte et al., 2017). For organic geochemistry, weight sub-aliquots were extracted as

225 described by Schreuder et al. (2018a). Shortly, ca. 100 mg dry weight of sediment trap residue, and

226 between 1.5 and 10 g of dry weight of surface sediment were extracted by ultrasonication using a mixture

227   of dichloromethane:methanol (DCM:MeOH) (2:1; v/v), and dried over a Na_2SO_4 column. For

228   quantification of LCDs, LCAs and GDGTs, we added the following internal standards to the total lipid

229   extracts (TLEs): 2.04 µg C_{22} 7,16 diol (Rodrigo-Gamiz et al., 2015), 1.50 µg 10-nonadecanone ($C_{19:0}$

230   ketone) and 0.1 µg C_{46} GDGT (Huguet et al., 2006), respectively. Subsequently, the TLEs were

231   separated into apolar (containing *n*-alkanes), ketone (containing LCAs) and polar (containing LCDs and

232   GDGTs) fractions over an activated (2h at 150 °C) Al_2O_3 column by eluting with hexane/DCM (9:1;

233   v/v), hexane/DCM (1:1; v/v) and DCM/MeOH (1:1; v/v), respectively. The apolar fractions were

234   analyzed by Schreuder et al. (2018a) for *n*-alkanes. Polar fractions were split for GDGT (25 %) and

235   LCD (75 %) analysis. The LCD fraction was silylated by the addition of BSTFA (*N*,*O*-

236   bis(trimethylsilyl)trifluoroacetamide) and pyridine, and heating at 60 °C for 20 min, after which ethyl

237   acetate was added prior to analysis. The ketone fraction was also dissolved in ethyl acetate, and the

238   GDGT fraction was dissolved in hexane:isopropanol (99:1, v/v) and analyzed by GC and GC/MS. Next,

239   the GDGT fractions were filtered through a 0.45 µm polytetrafluoroethylene (PTFE) filter and analyzed

240   by HPLC-MS.

241   **2.3.2 Mozambique Channel**

242   Aliquots of the sediment trap samples from the Mozambique Channel were previously extracted and

243   analyzed by Fallet et al. (2011) and Fallet et al. (2012), respectively. The sediment trap material was

244   extracted by ultrasonication using a mixture of DCM/MeOH (2:1; v/v), dried over Na_2SO_4, and

245   separated into apolar, ketone and polar fractions via alumina pipette column chromatography, by eluting

246   with hexane/DCM (9:1; v/v), hexane/DCM (1:1; v/v) and DCM/MeOH (1:1; v/v), respectively. These

247   existing polar fractions of the sediment trap material were silylated (as described above), dissolved in

248   ethyl acetate and re-analyzed for LCDs by GC-MS. Since no record was kept of the aliquoting of extracts

249   and polar fractions, we report the results in relative abundance rather than concentrations and fluxes of

250   diols.

251   **2.3.3 Cariaco Basin**

252   Sediment trap material was extracted as described by Turich et al. (2013). Briefly, 1/16 aliquots of the

253   trap samples were extracted by means of Bligh-Dyer extraction with sonication using a phosphate buffer

254   and a trichloroacetic acid (TCA) buffer, after which the extracts were separated by adding 5 % NaCl in

255   solvent-extracted distilled deionized water, and the organic phase was collected and the aqueous phase

256   was extracted two more times. The extracts were pooled and dried over Na_2SO_4 and separated by means

257   of Al_2O_3 column chromatography, eluting with hexane:DCM (9:1; v/v), DCM:MeOH (1:1; v/v) and

258   MeOH. For this study, this latter fraction was silylated (as described above), dissolved in ethyl acetate,

259   and analyzed for LCDs using GC-MS. Similar to the Mozambique Channel samples, no record was kept

260   of the aliquoting of extracts and polar fractions, and thus we report the results in relative abundance.

261

262   **2.4   Instrumental analysis**

263   **2.4.1 GDGTs**

264   The GDGT fractions of the surface sediments and sediment traps SPM samples of the tropical North

265   Atlantic were analyzed for GDGTs by means of Ultra High Performance Liquid Chromatography Mass

266   Spectrometry (UHPLC-MS). We used an Agilent 1260 HPLC, which is equipped with an automatic

267   injector, interfaced with a 6130 Agilent MSD, and HP Chemstation software according to Hopmans et

268   al. (2016). Compound separation was achieved by 2 silica BEH HILIC columns in tandem (150 mm x

269   2.1 mm; 1,7 µm; Waters Acquity) in normal phase, at 25 °C. GDGTs were eluted isocratically for 25

270   min with 18 % B, followed by a linear gradient to 35 % B in 25 minutes and finally a linear gradient to

271   100 % B in the last 30 min. A = hexane; B = hexane:isopropanol (9:1; v/v). The flow rate was constant

272   at 0.2 mL min^{-1}, and the injection volume was 10 µL. The APCI-MS conditions are described by

273   Hopmans et al. (2016). Detection and quantification of GDGTs was achieved in single ion monitoring

274   (SIM) mode of the protonated molecules ($[M+H]^+$) of the GDGTs. We used a mixture of crenarchaeol

275   and the C_{46} GDGT (internal standard) to assess the relative response factor, which was used for

276   quantification of the GDGTs in the samples (c.f. Huguet et al., 2006).

277   Sea surface temperatures were calculated by means of the TEX^H_{86} as defined by Kim et al. (2010), which

278   is a logarithmic function of the original TEX_{86} index (Schouten et al., 2002):

279        $$TEX^H_{86} = \log \frac{[GDGT-2] + [GDGT-3] + [Cren']}{[GDGT-1] + [GDGT-2] + [GDGT-3] + [Cren']}$$ [1]

280 where the numbers indicate the number of cyclopentane moieties of the isoprenoid GDGTs, and *Cren´*

281 reflects an isomer of crenarchaeol, i.e. containing a cyclopentane moiety with a *cis* stereochemistry

282 (Sinninghe Damsté et al., 2018). The TEX^H_{86} values were translated to SSTs using the core-top

283 calibration of Kim et al. (2010):

284 $$SST = 68.4 \times TEX^H_{86} + 38.6 \qquad [2]$$

285 The Branched Isoprenoid Tetraether (BIT) index is a proxy for the relative contribution of terrestrial

286 derived organic carbon (de Jonge et al., 2014; 2015). This ratio is based on the original index as proposed

287 by Hopmans et al. (2004), but includes the 6-methyl brGDGTs:

288 $$BIT = \frac{[brGDGT\ Ia] + [brGDGT\ IIa+IIa'] + [brGDGT\ IIIa+IIIa']}{[brGDGT\ Ia] + [brGDGT\ IIa+IIa'] + [brGDGT\ IIIa+IIIa'] + [Cren]} \qquad [3]$$

289 where the numbers reflect different branched GDGTs (see Hopmans et al., 2004) and *Cren* reflects

290 crenarchaeol. The branched GDGTs were always around the detection limit in the Atlantic samples,

291 implying a BIT index of around zero and thus minimal influence of soil organic carbon (Hopmans et al.,

292 2004), and thus the BIT index is not discussed any further.

293

294 ### 2.4.2 LCAs

295 The ketone fractions of the surface sediments and sediment traps samples of the tropical North Atlantic

296 were analyzed for LCAs on an Agilent 6890N gas chromatograph (GC) with flame ionization

297 detection (FID) after dissolving in ethyl acetate. The GC was equipped with a fused silica column with

298 a length of 50 m, a diameter of 0.32 mm, and a coating of CP Sil-5 (film thickness = 0.12 μm). Helium

299 was used as carrier gas, and the flow mode was a constant pressure of 100 kPa. The ketone fractions

300 were injected on-column at a starting temperature of 70 °C, which increased by 20 °C min^{-1} to 200 °C

301 followed by 3 °C min^{-1} until the final temperature of 320 °C was reached. This end temperature was

302 held for 25 min.

303 The $U^{K'}_{37}$ index was calculated according to Prahl and Wakeham (1987):

304 $$U^{K'}_{37} = \frac{[C_{37:2}]}{[C_{37:2}] + [C_{37:3}]} \qquad [4]$$

305   The $U^{K'}_{37}$ values were translated to SST after the calibration of Müller et al. (1998):

306    $$SST = \frac{U^{K'}_{37} - 0.044}{0.033}$$ [5]

307   We have also applied the recently proposed BAYSPLINE Bayesian calibration of Tierney and Tingley

308   (2018). The authors showed that the $U^{K'}_{37}$ estimates substantially attenuate above temperatures of 24 °C,

309   moving the upper limit of the $U^{K'}_{37}$ calibration from approximately 28 to 29.6 °C at unity. Since our

310   traps are located in tropical regions with SSTs > 24 °C, we have applied this calibration as well.

311

2.4.3   LCDs

313   The silylated polar fractions were injected on-column on an Agilent 7890B gas chromatograph (GC)

314   coupled to an Agilent 5977A mass spectrometer (MS). The starting temperature was 70 °C, and

315   increased to 130 °C by 20 °C min^{-1}, followed by a linear gradient of 4 °C min^{-1} to an end temperature of

316   320 °C, which was held for 25 min. 1μL was injected, and separation was achieved on a fused silica

317   column (25 × 0.32 mm) coated with CP Sil-5 (film thickness 0.12 μm). Helium was used as carrier gas

318   with a constant flow of 2 mL min^{-1}. The MS operated with an ionization energy of 70 eV. Identification

319   of LCDs was done in full scan mode, scanning between m/z 50–850, based on characteristic

320   fragmentation patterns (Volkman et al., 1992; Versteegh et al., 1997). Proxy calculations and LCD

321   quantifications were performed by analysis in SIM mode of the characteristic fragments (m/z 299, 313,

322   327 and 341; Rampen et al., 2012; m/z 187 for internal diol standard). For quantification of LCDs in the

323   sediment traps and seafloor sediments of the tropical Atlantic, the peak areas of the LCDs were corrected

324   for the average relative contribution of the selected SIM fragments to the total ion counts, i.e., 16 % for

325   the saturated LCDs, 9 % for unsaturated LCDs and 25 % for the C_{22} 7,16-diol internal standard.

326   Sea surface temperatures were calculated using the LDI index, according to Rampen et al. (2012):

327    $$LDI = \frac{[C_{30}\ 1,15-diol]}{[C_{28}\ 1,13-diol] + [C_{30}\ 1,13-diol] + [C_{30}\ 1,15-diol]}$$ [6]

328   These LDI values were converted into SSTs using the following equation (Rampen et al., 2012):

329 $$\text{SST} = \frac{\text{LDI} - 0.095}{0.033} \qquad [7]$$

330 Upwelling conditions were reconstructed using the Diol Index as proposed by Rampen et al. (2008):

331 $$\text{Diol Index} = \frac{[C_{28}\ 1,14-diol] + [C_{30}\ 1,14-diol]}{[C_{28}\ 1,14-diol] + [C_{30}\ 1,14-diol] + [C_{30}\ 1,15-diol]} \qquad [8]$$

332 In 2010, Willmott et al. introduced an alternative Diol Index, which is defined as the ratio of 1,14-diols

333 over 1,13-diols. Since the index of Rampen et al. (2008) includes the C_{30} 1,15-diol, it can be affected by

334 temperature variation, and therefore we would normally prefer to use the index of Willmott et al. (2010).

335 However, we often did not detect the C_{28} 1,13-diol, or it co-eluted with cholest-5-en-7-one-3β-ol,

336 compromising the calculation of the Diol Index of Willmott et al. (2010). Moreover, the temperature

337 variations in all three sediment traps are minimal as recorded by the LDI. Accordingly, we chose to

338 apply the Diol Index according to Rampen et al. (2008).

339 Potential fluvial input of organic carbon was determined by the fractional abundance of the C_{32} 1,15-

340 diol (de Bar et al., 2016; Lattaud et al., 2017a):

341 $$F\text{C}_{32}\ 1,15\text{-diol} = \frac{[C_{32}\ 1,15-diol]}{[C_{28}\ 1,13-diol] + [C_{30}\ 1,13-diol] + [C_{30}\ 1,15-diol] + [C_{32}\ 1,15-diol]} \qquad [9]$$

342 The fractional abundance of the C_{32} 1,15-diol was always lower than 0.23, suggesting low input of river

343 derived organic carbon (Lattaud et al., 2017a).

344

345 **2.5   Time-series analysis**

346 We performed time-series spectral analysis on the Diol Index data from the Mozambique Channel to

347 assess the influence of meso-scale eddies. Analyses were performed in MATLAB®. The two parts of

348 the Diol Index time series, i.e. the 2003–2007 and the 2008–2009 periods, were analysed both separately

349 and together. The data were linearly interpolated in time (to 21-day intervals for the 2003–2007 period,

350 and 17-day intervals for the 2008–2009 period) to adjust for disjunct sampling intervals or short gaps,

351 and detrended. A runs test for randomness (Gibbons & Chakraborty, 2003) showed that for the second,

352 shorter time series (2008–2009) the null hypothesis – that the values in the series are in random order –

353 could not be rejected at the 5 % significance level. The second series also lacked statistically significant

354 autocorrelation according to the Ljung-Box test (Ljung & Box, 1978). Therefore, there was little point

355 in analysing the shorter 2008–2009 time series for periodicity. We performed a wavelet analysis to detect

356 transient features in the Mozambique Channel Diol Index 2003–2007 time series following the methods

357 of Torrence and Compo (1998; http://paos.colorado.edu/research/wavelets/) and using the Morlet

358 wavelet as mother wavelet.

359

360 ### 3. Results

361 #### 3.1 Tropical North Atlantic

362 We have analyzed sediment trap samples from a latitudinal transect (~ 12°N) in the tropical North

363 Atlantic (two upper traps at ca. 1200 m water depth, and three lower traps at ca. 3500 m; Fig. 1), covering

364 November 2012–November 2013, as well as seven underlying surface sediments, for LCDs, LCAs and

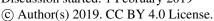365 GDGTs. Below we present the results for these lipid biomarkers and associated proxies.

366 #### 3.1.1 LCDs

367 The LCDs detected in the sediment trap samples and surface sediments from the tropical North Atlantic

368 (Fig. 2) are the C_{28} and (mono-unsaturated and saturated) C_{30} 1,14- (between 1 and 49 % of all LCDs),

369 C_{28} and C_{30} 1,13- (0–3 %) and the C_{30} 1,15- (44–99 %) and C_{32} 1,15-diols (0–7 %). In the M2 and M4

370 traps, the C_{30} 1,15-diol constitutes between 87 and 95 % of total LCDs. We detected the C_{29}-OH fatty

371 acid in the traps from M1 and M4, in a few samples of the M2 traps and in all surface sediments.

372 Similarly, the C_{28} 1,14-diol was detected in all samples from M1 and M4, in only a few M2 samples and

373 in all surface sediments. For most samples from M2U and M2L, the C_{28} 1,14-diol was often part of a

374 high background signal, making identification and quantification problematic. In these cases, 1,14-diol

375 fluxes and Diol Index were solely based on the (saturated and mono-unsaturated) C_{30} 1,14-diol. In

376 contrast, the saturated C_{30} 1,14-diol was detected in all samples.

377 The average [1,13+1,15]-diol flux is 2.6 (± 1.0) µg m^{-2} d^{-1} at M1U, 1.4 (± 1.2) and 1. 2 (± 1.1) µg m^{-2} d^{-}

378 ^{1} for M2U and M2L, respectively, and 7.0 (± 7.8) and 2.2 (± 3.3) µg m^{-2} d^{-1} for M4U and M4L,

379   respectively (Fig. 3). The [1,13+1,15]-diol and 1,14-diol concentrations in the underlying sediments

380   vary between 0.05 µg g^{-1} and 0.50 µg g^{-1}, and between 3 ng g^{-1} and 0.06 µg g^{-1}, respectively. The

381   [1,13+1,15]-LCD flux is more than three times higher in the upper trap of M4 than in the lower trap,

382   whereas at M2, where the average LCD fluxes are much lower, the difference is not appreciable. The

383   1,14-diol flux for M1U averages 0.5 ($\pm$ 0.8) µg m^{-2} d^{-1} with a pronounced maximum of 3.5 µg m^{-2} d^{-1} in

384   late April (Fig. 6a), irrespective of the total mass flux. The average 1,14-diol flux at M2 is much lower

385   and similar for the upper and lower traps, being around 0.01–0.02 ($\pm$ 0.01) µg m^{-2} d^{-1}. At M4, the average

386   1,14-diol fluxes are 0.3 ($\pm$ 0.5) and 0.1 ($\pm$ 0.2) µg m^{-2} d^{-1} for the upper and lower trap, respectively.

387   There are two evident maxima in the [1,13+1,15]-diols and 1,14-diol fluxes in late April and during

388   October/November, concomitant with maxima in the total mass flux (Fig. 3d and 3e). However, in the

389   lower trap this flux maximum is distributed over two successive trap cups, corresponding to late

390   April/early May (Fig. 3e and 3j).

391   The LDI ranged between 0.95 and 0.99 in all traps, corresponding to temperatures of 26.0 to 27.3 °C

392   with no particular trends (Fig. 5). For most M2 and M4 samples the C$_{28}$ 1,13-diol was below

393   quantification limit and, hence, LDI was always around unity, corresponding to 26.9 to 27.3 °C (Fig. 5),

394   whereas in others samples the C$_{28}$ 1,13-diol co-eluted with cholest-5-en-7-one-3β-ol, prohibiting the

395   calculation of the LDI and Diol Index (Fig. 5 and 6). The flux-weighted annual average LDI-derived

396   SSTs are 26.6 °C for M1U, and 27.1 °C for M2U, M2L, M4U and M4L. The underlying sediment is

397   very similar, with LDI values between of 0.95 and 0.98 corresponding to 26.0 and 26.9 °C. The Diol

398   Index varied from 0.03 to 0.30 in M1U, showing a pronounced maximum during spring (Fig. 6a). The

399   Diol Index at M2 ranges between 0.01 and 0.05 without an evident pattern, while the Diol Index at M4

400   ranges from 0.01 to 0.10 and shows the same pattern in the lower and upper trap, with highest values

401   during spring (ca. 0.1), followed by a gradual decrease during summer (Fig. 6d; 6e).

402

403   **3.1.2 LCAs**

404   We detected C$_{37}$, C$_{38}$ and C$_{39}$ long-chain alkenones in the sediment trap and surface sediments. The C$_{37:3}$

405   alkenone was generally around the limit of quantification for the M2L and M4L traps, and below the

406 limit of quantification for 4 out of the 7 surface sediment samples, while the $C_{37:2}$ alkenone was always

407 sufficiently abundant. The annual mean fluxes of the C_{37} LCAs are 4.3 ($\pm$ 3.5) µg m^{-2} d^{-1} for M1U, 1.2

408 ($\pm$ 0.9) µg m^{-2} d^{-1} and 0.4 ($\pm$ 0.2) µg m^{-2} d^{-1} for M2U and M2L, respectively, and 2.8 ($\pm$ 5.0) µg m^{-2} d^{-1}

409 and 1.2 ($\pm$ 2.0) µg m^{-2} d^{-1} for M4U and M4L, respectively. The concentrations of the C_{37} LCAs in the

410 underlying surface sediments range between 0.02 and 0.41 µg g^{-1}. At M4, the two total mass flux peaks

411 at the end of April and during October/November are also clearly pronounced in the C_{37} alkenone fluxes

412 (Fig. 3d, 3e and 6g), as well as the increased signal in the cup reflecting the beginning of May, which

413 follows the cup which recorded the peak in total mass flux at the end of April. The $U^{K'}_{37}$ varied from

414 0.87 to 0.93, corresponding to 25.1 to 27.0 °C (Fig. 7c) for 3 out of 7 surface sediments in which the

415 $C_{37:3}$ was above quantification limit. The flux-weighted average SSTs are 26.1 °C for M1U, 25.7 and

416 26.4 °C for M2U and M2L, respectively, and 28.2 and 27.5 °C for M4U and M4L, respectively (Fig. 7).

417 SST variations per sediment trap are generally within a 2–3 °C range (Fig. 5) with no apparent trends.

418

419 **3.1.3 GDGTs**

420 The main GDGTs detected were the isoprenoidal GDGT-0, -1, -2, -3, crenarchaeol and the isomer of

421 crenarchaeol. Branched GDGTs were typically around or below quantification limit. Additionally, we

422 detected three hydroxyl GDGTs (OH-GDGTs), i.e. OH-GDGT-0, -1 and -2. These OH-GDGTs

423 contributed ca. 0.1–0.2 % to the total GDGT pool (i.e., hydroxyl and isoprenoidal) in the sediment traps,

424 but in the surface sediments their fractional abundance was higher, around 1 %. The average iGDGT

425 flux in M1U is 15.5 ($\pm$ 4.6) µg m^{-2} d^{-1}, 2.4 ($\pm$ 1.1) and 2.6 ($\pm$ 0.3) µg m^{-2} d^{-1} in M2U and M2L,

426 respectively, and 4.3 ($\pm$ 1.5) and 2.9 ($\pm$ 1.2) µg m^{-2} d^{-1} in M4U and M4L, respectively (Fig. 3f). The

427 surface sediments exhibit iGDGT concentrations between 0.4 and 1.7 µg g^{-1}. Sediment TEX$^H_{86}$ values

428 vary between 0.62 and 0.69, corresponding to 24.3 to 27.4 °C. The TEX$^H_{86}$ flux-weighted average SSTs

429 are 25.2 °C for M1U, 27.3 and 26.6 °C for M2U and M2L, respectively, and 27.8 and 26.7 °C for M4U

430 and M4L, respectively. SSTs vary typically within a range of 1 and 2 °C. At M2U and M4U, the TEX$^H_{86}$

431 temperatures decrease slightly (ca. 1–2 °C) during January and July (Fig. 5b and 5d).

432

3.2 Mozambique Channel

For two time series (November 2003–September 2007 and February 2008–February 2009), we have analyzed LCDs collected in the sediment trap at 2250 m water depth as well as nearby underlying surface sediments (Fig. 1). The main LCDs observed in the sediment traps and surface sediments are the C_{28} 1,12-, 1,13- and 1,14-diols, the C_{30} 1,13-, 1,14- and 1,15-diols and the C_{32} 1,15-diol. We also observed the $C_{30:1}$ 1 1,14 diol in some trap samples, and the C_{29} 12-OH fatty acid in all trap and sediment samples. The C_{30} 1,15 is generally highest in abundance, varying between 28 and 85 % of the total LCD assemblage. The C_{28} and C_{30} 1,14-diols contribute between 11 and 67 % of total LCDs. In 24 samples, the C_{28} 1,13-diol co-eluted with cholest-5-en-7-one-3β-ol, and henceforth we did not calculate the LDI for these samples. The LDI varied between 0.94 and 0.99, i.e., close to unity, corresponding to 25.5 to 27.2 °C, without an evident trend (Fig. 8a). The Diol Index ranges between 0.11 and 0.69, showing substantial variation, although not with an evident trend (Fig. 8b). The average LDI-derived temperature of two underlying surface sediments is 26.0 °C.

3.3 Cariaco Basin

We analyzed LCDs for two time series (May 1999–May 2000 and July 2002–July 2003) from the upper (Trap A; 275 m) and the lower trap (Trap B; 455 m) in the Cariaco Basin. The main LCDs detected for both time series are the C_{28} 1,14-, C_{30} 1,14-, $C_{30:1}$ 1,14-, C_{28} 1,13-, C_{30} 1,15- and C_{32} 1,15-diols, as well as the C_{29} 12-OH fatty acid. The C_{30} 1,15-diol contribution varies between 3 and 92 % of all LCDs, the C_{28} and C_{30} 1,14-diol contribution between 3 and 96 %, and the C_{28} and C_{30} 1,13-diols constitute between 0 and 8 %. For some samples we did not compute the LDI, as the C_{28} 1,13-diol co-eluted with cholest-5-en-7-one-3β-ol. The calculated LDI values range between 24.3 and 25.3 °C and 22.0 and 27.2 °C for Trap A and B of the 1999-2000 time series, respectively, with the lowest temperature during winter, and the highest during summer. For the 2002-2003 time series, LDI temperatures for Trap A range between 23.3 and 26.2 °C, and for Trap B between 22.5 °C and 26.5 °C.

458 For the May 1999–May 2000 time series, the Diol Index varies between 0.05 and 0.97 for Trap A, and

459 between 0.05 and 0.91 for Trap B (Fig. 9) with similar trends, i.e. the lowest values of around 0.1-0.2

460 just before the upwelling period during November, rapidly increasing towards values between ca. 0.8

461 and 1 during the upwelling season (January and February). For the time series of July 2002–July 2003,

462 the Diol Index shows similar trends, i.e. Diol Index values around 0.8-0.9 during July, which rapidly

463 decrease towards summer values of around 0.2-0.3. Similar to the 1999-2000 time series, the lowest

464 index values (ca. 0.2) are observed just before the upwelling period (during September), after which

465 they increase towards values of around 0.8-0.9 between December and March at the start of the

466 upwelling season. At the end of the upwelling season the Diol Index increases, followed by another

467 maximum of around 0.6 during May.

468 **4. Discussion**

469 **4.1 LCD sources and seasonality**

470 The 1,14 diols can potentially be derived from two sources, i.e. *Proboscia* diatoms (Sinninghe Damsté

471 et al., 2003; Rampen et al., 2007) or the dictyochophyte *Apedinella radians* (Rampen et al., 2011). The

472 non-detection of the C_{32} 1,14-diol, which is a biomarker for *Apedinella radians* (Rampen et al., 2011),

473 and the detection of the $C_{30:1}$ 1,14 diol and C_{29} 12-OH fatty acid, which are characteristic of *Proboscia*

474 diatoms (Sinninghe Damsté et al., 2003), suggests that *Proboscia* diatoms are most likely the source of

475 1,14-diols in the tropical North Atlantic, the Mozambique Channel and the Cariaco Basin.

476 In the Cariaco Basin, the Diol Index shows a strong correlation with primary production rates,

477 suggesting that *Proboscia* productivity was synchronous with total productivity (Fig. 9). Primary

478 productivity in the Cariaco Basin is largely related to seasonal upwelling which occurs between

479 November and May when the ITCZ is at its southern position. Hence, the Diol Index seems to be an

480 excellent indicator of upwelling intensity in the Cariaco Basin.

481 The index also shows considerable variation over time in the Mozambique Channel (Fig. 8b). Previous

482 studies have shown that upwelling occurs in the Mozambique Channel between ca. 15 and 18° (Nehring

483 et al., 1987; Malauene et al., 2014), i.e. at the location of our sediment trap. Upwelling is reflected by

484   cool water events and slightly enhanced Chlorophyll *a* levels, and Malauene et al. (2014) observed cool

485   water events at ca. two month intervals although periods of 8 to 30 days were also observed. The two

486   main potential forcing mechanisms for upwelling in the Mozambique Channel are the East African

487   monsoon winds and the meso-scale eddies migrating through the channel. Fallet et al. (2011) showed

488   that subsurface temperature, current velocity and the depth of surface-mixed layer all revealed a

489   dominant periodicity of four to six cycles per year, which is the same frequency as that of the southward

490   migration of meso-scale eddies in the channel (Harlander et al., 2009; Ridderinkhof et al., 2010),

491   implying that eddy passage strongly influences the water mass properties. Wavelet analysis of the Diol

492   Index for the period 2003–2007 (not shown) revealed short periods, occurring around January of 2004,

493   2005, and 2006, of significant (above the 95 % confidence level) variability at about bimonthly

494   frequencies (60-day period). Both the frequency and the timing of the observed time periods of enhanced

495   Diol Index variability are similar to those of the cool water events as observed by Malauene et al. (2014),

496   associated with upwelling (Fig. 8b). The strongest variability of the Diol Index at frequencies of four

497   cycles per year and higher occurred in the first half of 2006. During the same period, salinity time series

498   showed the passage of several eddies that had a particularly strong effect on the upper layer hydrography

499   (Ullgren et al., 2012). Malauene et al. (2014) showed that neither upwelling-favorable winds, nor

500   passing eddies, can by themselves explain the observed upwelling along the northern Mozambique

501   coast. The two processes may act together, and both strongly influence the upper water layer and the

502   organisms living there, potentially including the LCD producers.

503   The least (seasonal) variation in the Diol Index is observed at M2 in the tropical North Atlantic (Fig. 6b

504   and 5c), which is likely due to its central open ocean position, associated with relatively stable,

505   oligotrophic conditions (Guerreiro et al., 2017). In contrast, M4 and M1 are closer to the south American

506   and west African coast, respectively, and thus are potentially under the influence of Amazon river runoff

507   and upwelling, respectively, and specific wind and ocean circulation regimes (see Sect. 2.1.1). However,

508   at M4, the Diol Index is also low (max. 0.1), suggesting low *Proboscia* productivity (Fig. 6d and 5e).

509   At M1, by contrast, we observe enhanced values for the Diol Index of up to ~0.3 during spring (Fig. 6a).

510   Most likely, an upwelling signal at this location is associated with the seasonal upwelling of the Guinea
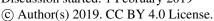
511   Dome. This upwelling is generally most intense between July and October (Siedler et al., 1992), due to

512   the northward movement of the ITCZ and the resulting intensified Ekman upwelling. Specifically,

513   during this period, the trade winds are weaker, atmospheric pressure is lower, and the regional wind

514   stress is favorable to upwelling of the North Equatorial Undercurrent (Voituriez, 1981). Indeed, a

515   decrease in wind speed and increased precipitation during summer to autumn was observed (Fig. 6a)

516   which confirms that during these seasons the ITCZ was indeed at a northern position, and that during

517   2013 the upwelling associated with the Guinea Dome was most favored between July and October. The

518   timing of the Diol Index peak, i.e., between March and June is consistent with previous sediment trap

519   studies elsewhere which have shown that *Proboscia* diatoms and 1,14-diols are typically found during

520   pre-upwelling or early upwelling periods (Koning et al., 2001; Smith, 2001; Sinninghe Damsté et al.,

521   2003; Rampen et al., 2007). The surface sediment at 22° W just east of M1 also reveals the highest Diol

522   Index (0.53), likely due its closer vicinity to the Guinea Dome center. Several studies have reported *P.*

523   *alata* diatoms offshore NW Africa (Lange et al., 1998; Treppke et al., 1995; Crosta et al., 2012; Romero

524   et al., 1999), pointing to *P. alata* as a plausible source organism. The sedimentary annual diol indices

525   compare well with the sediment trap indices (Fig. 7e), which is consistent with the results of Rampen et

526   al. (2008).

527   To assess variations in seasonal production of 1,13- and 1,15-diols in the tropical Atlantic, for which we

528   have the most complete dataset, we calculated the flux-weighted 1,13- and 1,15-diol concentrations for

529   the different traps, and summed these per season (Fig. 4). Highest production is observed in autumn,

530   followed by summer and spring, with the lowest production during winter (~60 % compared to autumn).

531   This is in agreement with Rampen et al. (2012) who observed, for an extensive set of surface sediments,

532   the strongest correlation between LDI and SST for autumn, suggesting that production of the source

533   organisms of the LDI mainly occurs during autumn. At M4, there are two evident peaks in the 1,13- and

534   1,15-diol fluxes at the end of April and October 2013. These maxima correlate with peaks in other lipid

535   biomarker fluxes (i.e., 1,14-diols, C_{37} alkenones and iGDGTs), total mass flux, calcium carbonate

536   ($CaCO_3$), OM and the residual mass flux which includes the deposition flux of Saharan dust (Korte et

537   al., 2017). According to Guerreiro et al. (2017), the maximum in total mass flux at the end of April 2013

538   is likely caused by enhanced export production due to nutrient enrichment as a result of wind-forced

539   vertical mixing. The peak at the end of October 2013, is likely associated with discharge from the

540   Amazon River. Moreover, both peaks are concomitant with prominent dust flux maxima, suggesting

541   that Saharan dust also acted as nutrient fertilizer (Korte et al., 2017; Guerreiro et al., 2017). Guirreirro

542   et al. (2017) suggested that during the October-November event the Amazon River may not only have

543   acted as nutrient supplier, but also as buoyant surface density retainer of dust-derived nutrients in the

544   surface waters, resulting in the development of algal blooms within just a few days, potentially

545   explaining the peak 1,13- and 1,15-diol fluxes, as well as the peak fluxes of the other lipid biomarkers.

546   However, they might also partially result from enhanced particle settling, caused by e.g. dust ballasting

547   or faecal pellets of zooplankton (see Guerreiro et al. 2017 and references therein). This agrees with the

548   results of Schreuder et al. (2018a) who show that the *n*-alkane flux also peaks concomitant with the

549   peaks in total mass flux and biomarkers, whereas *n*-alkanes are terrestrial derived (predominantly

550   transported by dust) and increased deposition can therefore not result from increased primary

551   productivity in the surface waters.

552   The C_{37} alkenone flux at M4U also reveals these two distinct maxima at the end of April and October

553   during 2013 (Fig, 6g). Interestingly, this flux, as well as the alkenone flux at M2U, is consistent with

554   coccolith export fluxes of the species *Emiliania huxleyi* and *Gephyrocapsa oceanica* (Guerreiro et al.,

555   2017). In fact, when we combine the coccolith fluxes of both species, we observe strong correlations

556   with the C_{37} alkenone fluxes for both M2U and M4U (Fig. 6f and 6g, respectively; $R^2 = 0.60$ and 0.84

557   for M2U and M4U, respectively). This implies that these two species are the main LCA producers in

558   the tropical North Atlantic, which agrees with previous findings (e.g., Marlowe et al., 1984; Brassell,

559   2014; Conte et al., 1994; Volkman et al., 1995).

560

561   **4.2 Preservation of LCDs**

562   The sediment trap data from the North Atlantic can be used to assess the relative preservation of LCDs,

563   as well as other proxy lipid biomarkers, by comparing the flux-weighted concentration in the traps with

564   the concentrations in the surface sediments. For all four biomarker groups, i.e., C_{37} alkenones, iGDGTs,

565 1,14-diols and 1,13- and 1,15-diols, we observe that in general the flux-weighted concentrations are

566 higher in the upper traps (ca. 1200 m) as compared to the lower traps (ca. 3500 m; Fig. 2) by a factor of

567 between 1.2 and 4.4, implying degradation during settling down the water column. The concentrations

568 in the surface sediments are 2 to 3 orders of magnitude lower in concentration (i.e., between 0.1–1.5 %

569 of upper trap signal), implying that degradation of lipids is mainly taking place at the water-sediment

570 surface rather than the water column. A similar observation was made for levoglucosan in these sediment

571 traps (Schreuder et al., 2018b). This is likely linked to the extent of the oxygen exposure time (Hartnett

572 et al., 1998; Hedges et al., 1999) at the seafloor (Hartnett et al., 1998; Sinninghe Damsté et al., 2002),

573 since during settling the lipids are exposed to oxygen for weeks, whereas for surface sediments this is

574 typically decades to centuries. Our results compare well with several other sediment trap studies which

575 showed that LCDs, LCAs and iGDGTs generally have a preservation factor of around 1 % (surface

576 sediment vs. trap) (e.g., Prahl et al., 2000; Wakeham et al., 2002; Rampen et al., 2007; Yamamoto et al.,

577 2012).

578 We have also identified the C_{30} and C_{32} 1,15-keto-ol for in the Atlantic as well as the Mozambique and

579 Cariaco sediment traps and surface sediments. These lipids are structurally related to LCDs and occur

580 ubiquitously in marine sediments (e.g., Versteegh et al., 1997; 2000; Bogus et al., 2012; Rampen et al.,

581 2007; Sinninghe Damsté et al., 2003; Wakeham et al., 2002; Jiang et al., 1994), and were inferred to be

582 oxidation products of LCDs (Ferreira et al., 2001; Bogus et al., 2012; Sinninghe Damsté et al., 2003).

583 We have not detected 1,14-keto-ols, which supports the hypothesis of Ferreira et al. (2001) and

584 Sinninghe Damsté et al. (2003) that the silica frustules of *Proboscia* diatoms sink relatively fast and thus

585 are exposed to oxygen for a shorter period than the 1,13- and 1,15-diols, and thus less affected by

586 oxidation.

587 For both the tropical Atlantic and the Cariaco Basin, we observe highly similar LDI values for the upper

588 and the lower traps. In the Atlantic there is no statistical difference between upper and lower trap that

589 are 2200 m apart (two-tailed $p > 0.8$), but we have too little data for the Cariaco Basin for statistical

590 comparison (Fig. 7b, 9c and 9f). This suggests that degradation in the water column does not affect the

591 LDI proxy. This is in agreement with the study of Reiche et al. (2018) who performed a short-term

592   degradation experiment (< 1 year) and found that the LDI index was not affected by oxic exposure on

593   short time scales. However, the oxygen exposure time on the seafloor is much longer, and Rodrigo-

594   Gámiz et al. (2016) showed for sediments in the Arabian Sea, deposited under a range of bottom water

595   oxygen conditions, that different LCDs had different degradation rates, which compromised the LDI

596   ratio. For the three sites in the tropical North Atlantic, we have calculated the flux-weighted average

597   proxy values for every sediment trap and compare these with the underlying surface sediments (Fig. 7b-

598   7e). For all indices, i.e., Diol Index, LDI, $U^{K'}_{37}$ and TEX_{86}, we observe very good correspondence

599   between the sediment trap and surface sediment values, implying minimal alteration of the proxies after

600   settling and during burial. Similarly, for the Mozambique Channel, the mean Diol Index and LDI from

601   the sediment trap (i.e., 0.41 and 0.97, respectively) are very similar to the surface sediment values (i.e.,

602   0.42 and 0.95, respectively). In agreement with the consistent diol indices, we observe that all individual

603   LCDs are also preserved relatively equally in the tropical Atlantic (1.2-4.3 % at station M1, 0.1-2.9 %

604   at station M2 and 0.03-0.16 % at station M4). This contrasts with the findings of Rodrigo-Gámiz et al.

605   (2016) who found that the 1,15-diols have the highest degradation rate, followed by the 1,14- and 1,13-

606   diols. Only the C_{32} 1,15-diol seems relatively better preserved than the other LCDs at all three North

607   Atlantic mooring sites (Fig. 2), suggesting that the C_{32} 1,15-diol is less impacted by degradation. The

608   C_{32} 1,15-diol likely partially derives from the same source as the other 1,13- and 1,15-diols, but is also

609   produced in fresh water systems (e.g., Versteegh et al., 1997; 2000; Rampen et al., 2014b; de Bar et al.,

610   2016; Lattaud et al., 2017a; 2017b). Hence, the different preservation characteristics might be the result

611   of a different source for this LCD.

612

4.3 Relationship between LDI and SST

614   In the tropical Atlantic and Mozambique Channel, the LDI-derived SSTs show minimal differences (<2

615   °C), while in the Cariaco Basin we observe much larger changes that range from 22.0 °C to 27.2 °C

616   (Fig. 9). Both time series in the Cariaco Basin show low temperatures between November and May

617   associated with the seasonal upwelling and surface water cooling, and significantly higher temperatures

618   during the rainy summer. However, during the warmest periods, the LDI temperatures are generally

619   lower than measured at the surface by CTD, whereas during the colder phases, the LDI agrees well with

620   the measurements. The LDI calibration reaches unity at 27.4 °C, and therefore it is not possible to resolve

621   the highest temperatures which are between ca. 28 and 30 °C. However, the LDI-derived temperatures

622   are sometimes well below 27.4 °C where the CTD data suggest SSTs > 28 °C. Consequently, the LDI-

623   based temperatures agree with CTD-based SSTs within calibration error for most of the record, but

624   during summer when SST is highest, are offset outside the calibration error (ΔT ~2.5-4.5 °C).

625   Interestingly, the $U^{K'}_{37}$- and TEX^{H}_{86}-derived temperature trends show the same phenomenon (Turich et

626   al., 2013; Fig. 9), where the proxy temperatures are cooler than the measured temperatures during the

627   warmer months. For $U^{K'}_{37}$, Turich et al. (2013) pointed out that a time lag between synthesis, export and

628   deposition could potentially explain the difference between the proxy and CTD temperatures. However,

629   previous analysis of plankton biomass, primary productivity, bio-optical properties and particulate

630   organic carbon fluxes for the same time period (Müller-Karger et al., 2004), as well as the total mass

631   and terrigenous fluxes assessed by Turich et al. (2013) showed best correlation at zero-time lag on the

632   basis of their 14-day sample interval. We compared our LDI temperature estimates with monthly CTD

633   measurements between 0 and 50 m depth, the temperature at depth of maximum primary productivity

634   and the temperature at the chlorophyll maximum (Turich et al., 2013; http://www.imars.usf.edu/cariaco)

635   (Fig. 10). During the upwelling season, temperatures are significantly lower due to the upward migration

636   of isotherms, whereas during the non-upwelling period, temperatures are higher, particularly in the upper

637   20 m, and the water column is more stratified (Fig. 10). LDI underestimates SST during stratification,

638   which suggests that the LCD producers may thrive at depths of ca. 20–30 m. During upwelling, LDI-

639   temperatures agree better with SST, implying that the habitat of the LCD producers potentially was

640   closer to the surface, coincident with the shoaling of the nutricline and thermocline (Fig. 10). Turich et

641   al. (2003) found that the $U^{K'}_{37}$-derived temperatures agreed reasonably well with the measured

642   temperatures at the chlorophyll maximum, which is generally found below 20 m depth (average 30–34

643   m depth; ranging between 1 and 55 m) in the Cariaco Basin. The LDI temperatures are almost always

644   higher than the temperatures at the chlorophyll maximum (Fig. 10), and higher than the temperatures at

645   30 m depth, implying that the LDI producers may reside in the upper 30 m of the water column, which

646   is consistent with the results of Rampen et al. (2012), who showed that LDI-derived temperatures have

647   the strongest correlation with temperatures of the upper 20 m of the water column. This also agrees with
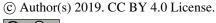
648   Balzano et al. (2018) who observed highest LCD abundances within the upper 20 m of the water column

649   in the Tropical Atlantic.

650   In the Mozambique Channel, the LDI temperature variations are much smaller (< 2 °C; Fig. 8a) than the

651   seasonal SST variation ranging between ca. 24.5 and 30.5 °C. Accordingly, during the warmest months

652   of the year, the difference between LDI-derived and satellite-derived SST is outside of the calibration

653   error (i.e., > 2 °C). However, this is similar to the $U^{K'}_{37}$ and TEX^H_{86} which also did not reveal seasonal

654   variations. This lack of seasonality was explained by lateral advection and re-suspension of fine

655   sediment material by migrating meso-scale eddies and thus ending up in the deeply moored sediment

656   trap (Fallet et al., 2011; 2012). Most likely, this also explains the lack of seasonal variation in our LDI

657   record (Fig. 8a). Nevertheless, the average LDI temperature for the sediment trap of 26.4 °C agrees

658   reasonably well with the annual mean satellite-derived SST of 27.6 °C for the sampled years.

659   Additionally, there is a good agreement with the average LDI temperature of 26.0 °C for two underlying

660   surface sediments, as well as with the decadal average SST of 26.7 °C for 1955-2012 (Locarnini et al.,

661   2013) given by the World Ocean Atlas (2013). For the North Atlantic, we also observe rather constant

662   LDI temperatures during the year (Fig. 5) which contrasts with seasonal variations in satellite SSTs of

663   ca. 3 to 5 °C. Nevertheless, differences are mostly within the calibration error, except at M1 and M2

664   where during winter and spring LDI-derived temperatures are between 0.5 and 2.8 °C higher than

665   satellite SSTs. Similar to the LDI, also the TEX^H_{86} and $U^{K'}_{37}$-derived SSTs for the tropical Atlantic

666   sediment traps do not reveal clear seasonal variation. As all three proxies show minimal seasonal

667   variability, this might indicate that the lipids are potentially allochtonous and partially derive from

668   distant regions, resulting in an integrated average temperature signal, similar to the Mozambique

669   Channel. Nevertheless, the flux-weighted annual LDI temperatures of the tropical Atlantic sediment

670   traps (26.6 for M1 and 27.1 °C for M2 and M4) agree well with the annual mean satellite-derived SSTs

671   of 26.1, 26.0 and 27.5 °C for M1, M2 and M4, respectively. Moreover, the LDI-derived temperatures in

672   the underlying sediments (26.5, 26.6 and 26.7 °C, respectively) do not only agree well with those found

673   in a single year in the sediment traps but also with the decadal average SSTs for 1955 to 2012 (26.2,

674   27.1 and 26.3 °C, respectively; Locarnini et al., 2013; Fig. 7b).

675

676   Interestingly, TEX^H_{86} temperature estimates are relatively similar for traps M2 and M4 but at M1 they

677   are lower than satellite SST in both the sediment trap and surface sediments (Fig. 7d). This

678   underestimation of SST at M1 might suggest GDGT addition from colder subsurface waters. Indeed

679   Balzano et al. (unpublished results) show that crenarchaeol is typically abundant between ca. 40 and

680   100 m water depth, agreeing with previous findings which have shown that the TEX_{86} can reflect

681   subsurface temperatures rather than surface temperature in some regions (e.g., Huguet et al., 2007; Kim

682   et al., 2012; 2015; Schouten et al., 2013; Chen et al., 2014; Wuchter et al., 2006). Consequently, for the

683   surface sediments, we also calculated subsurface temperatures, using the calibration of Kim et al. (2012)

684   (Fig. 7d), and compared these with the depth-integrated annual mean temperatures of the upper 150 m

685   (Locarnini et al., 2013), caclulated following Kim et al. (2008), which indeed shows a better

686   correspondence for the eastern Atlantic surface sediment, i.e., the sediments close to M1. This is likely

687   caused by the steepening of the thermocline towards the east, as shown in Fig. 7a,d, in which we have

688   indicated the approximate production depths of the temperature proxies. The thermocline at M1 is much

689   steeper and shallower, which implies that GDGTs produced at ~ 100 m depth will record a lower

690   temperature than at M2 and M4.

691

692   **5. Conclusions**

693   In this study we have evaluated LCD-based proxies, particularly the LDI, in sediment trap time series

694   from five sites in the tropical North Atlantic, the Cariaco Basin and the Mozambique Channel. For the

695   North Atlantic we found that in the water column ca. 25–85 % of the export of these lipid biomarkers is

696   preserved during settling from 1200m to 3500m, and that generally less than 2 % was preserved in the

697   surface sediments. Despite substantial degradation at the seafloor, likely linked to the prolonged oxygen

698   exposure time, LCD-derived temperatures from the sediments are generally very similar to the annual

699   mean LCD-derived temperatures in both the deep and shallow traps as well as to annual mean SST for

700   the specific sampling year and on decadal time scales for the specific sites. In the Cariaco Basin we

701   observe a strong seasonality in the LDI which is linked to the upwelling season at temperatures

702   associated with a water depth of up to ca. 30 m during summer stratification, and at SST during winter

703   upwelling accompanied by shoaling of both the nutricline and isotherms. The LDI temperatures in the

704   Mozambique Channel and the tropical Atlantic reveal minimal seasonal change although seasonal SST

705   contrasts amount to 3-5°C. For the Mozambique Channel this is likely caused by lateral advection of re-

706   suspended sediment by meso-scale eddy migration, a signal not substantially altered by diagenesis.

707   Seasonal variations in the Diol Index are minimal in the central and western North Atlantic and 1,14-

708   diol concentrations are rather low, implying little *Proboscia* diatom productivity. However, in the

709   eastern Atlantic closest to the African continent, the Diol Index attains a clear spring maximum that is

710   likely associated with upwelling in the Guinea Dome during summer to autumn, suggesting the Diol

711   Index reflects a pre-upwelling signal, consistent with the current knowledge on *Proboscia* ecology. In

712   the Cariaco Basin, controlled by seasonal upwelling, the Diol Index reveals the same clear seasonal

713   trend observed in primary productivity, arguing that for this location the Diol Index is an excellent

714   indicator of upwelling intensity.

715

716   **Data availability**. The data reported in this paper is archived in PANGAEA (www.pangaea.de.)

717

718   **Author contributions**. MWdB, JSSD, and SS designed the experiments and MWdB carried them out.

719   JU carried out the time-series analysis. JBWS, GJAB, and RCT deployed sediment traps and collected

720   sediment trap materials. MWdB prepared the paper with contributions from coauthors.

721

722   **Competing interests**. The authors declare that they have no conflict of interest.

723

733

734 **References**

735   Araujo, M., Noriega, C., Hounsou-gbo, G. A., Veleda, D., Araujo, J., Bruto, L., Feitosa, F.,

736 Flores-Montes, M., Lefevre, N., Melo, P., Otsuka, A., Travassos, K., Schwamborn, R., and Neumann-

737 Leitao, S.: A Synoptic Assessment of the Amazon River-Ocean Continuum during Boreal Autumn:

738 From Physics to Plankton Communities and Carbon Flux, Front. Microbiol., 8,

739 https://doi.org/10.3389/fmicb.2017.01358, 2017.

740   Balzano, S., Lattaud, J., Villanueva, L., Rampen, S. W., Brussaard, C. P. D., van Bleijswijk, J.,

741 Bale, N., Sinninghe Damsté, J. S., and Schouten, S.: A quest for the biological sources of long chain

742 alkyl diols in the western tropical North Atlantic Ocean, Biogeosciences, 15, 5951-5968,

743 https://doi.org/10.5194/bg-15-5951-2018, 2018.

744   Biastoch, A., and Krauss, W.: The Role of Mesoscale Eddies in the Source Regions of the

745 Agulhas Current, J. Phys. Oceanogr., 29, 2303-2317, https://doi.org/10.1175/1520-

746 0485(1999)029<2303:Tromei>2.0.Co;2, 1999.

747   Bogus, K. A., Zonneveld, K. A. F., Fischer, D., Kasten, S., Bohrmann, G., and Versteegh, G. J.

748 M.: The effect of meter-scale lateral oxygen gradients at the sediment-water interface on selected

749 organic matter based alteration, productivity and temperature proxies, Biogeosciences, 9, 1553-1570,

750 https://doi.org/10.5194/bg-9-1553-2012, 2012.

751   Brassell, S. C., Eglinton, G., Marlowe, I. T., Pflaumann, U., and Sarnthein, M.: Molecular

752   stratigraphy – A new tool for climatic assessment, Nature, 320, 129-133,

753   https://doi.org/10.1038/320129a0, 1986.

754   Brassell, S. C.: Climatic influences on the Paleogene evolution of alkenones, Paleoceanography,

755   29, 255-272, https://doi.org/10.1002/2013pa002576, 2014.

756   Chen, W. W., Mohtadi, M., Schefuss, E., and Mollenhauer, G.: Organic-geochemical proxies

757   of sea surface temperature in surface sediments of the tropical eastern Indian Ocean, Deep-Sea Res. Pt.

758   I, 88, 17-29, https://doi.org/10.1016/j.dsr.2014.03.005, 2014.

759   Coles, V. J., Brooks, M. T., Hopkins, J., Stukel, M. R., Yager, P. L., and Hood, R. R.: The

760   pathways and properties of the Amazon River Plume in the tropical North Atlantic Ocean, J. Geophys.

761   Res-Oceans, 118, 6894-6913, https://doi.org/10.1002/2013jc008981, 2013.

762   Conte, M. H., Thompson, A., and Eglinton, G.: Primary production of lipid biomarker

763   compounds by *Emiliania Huxleyi* – Results from an experimental mesocosm study in fjords of

764   southwestern Norway, Sarsia, 79, 319-331, https://doi.org/10.1080/00364827.1994.10413564, 1994.

765   Conte, M. H., Sicre, M. A., Ruhlemann, C., Weber, J. C., Schulte, S., Schulz-Bull, D., and

766   Blanz, T.: Global temperature calibration of the alkenone unsaturation index $U^{K'}_{37}$ in surface waters and

767   comparison with surface sediments, Geochem. Geophy. Geosy., 7,

768   https://doi.org/10.1029/2005GC001054, 2006.

769   Cropper, T. E., Hanna, E., and Bigg, G. R.: Spatial and temporal seasonal trends in coastal

770   upwelling off Northwest Africa, 1981-2012, Deep-Sea Res. Pt. I, 86, 94-111,

771   https://doi.org/10.1016/j.dsr.2014.01.007, 2014.

772   Crosta, X., Romero, O. E., Ther, O., and Schneider, R. R.: Climatically-controlled siliceous

773   productivity in the eastern Gulf of Guinea during the last 40 000 yr, Clim. Past, 8, 415-431,

774   https://doi.org/10.5194/cp-8-415-2012, 2012.

775   de Bar, M. W., Dorhout, D. J. C., Hopmans, E. C., Rampen, S. W., Sinninghe Damsté, J. S., and

776   Schouten, S.: Constraints on the application of long chain diol proxies in the Iberian Atlantic margin,

777   Org. Geochem., 101, 184-195, https://doi.org/10.1016/j.orggeochem.2016.09.005, 2016.

778   de Jonge, C., Hopmans, E. C., Zell, C. I., Kim, J. H., Schouten, S., and Sinninghe Damsté, J. S.:

779   Occurrence and abundance of 6-methyl branched glycerol dialkyl glycerol tetraethers in soils:

780   Implications for palaeoclimate reconstruction, Geochim. Cosmochim. Ac., 141, 97-112,

781   https://doi.org/10.1016/j.gca.2014.06.013, 2014.

782   de Jonge, C., Stadnitskaia, A., Hopmans, E. C., Cherkashov, G., Fedotov, A., Streletskaya, I.

783   D., Vasiliev, A. A., and Sinninghe Damsté, J. S.: Drastic changes in the distribution of branched

784   tetraether lipids in suspended matter and sediments from the Yenisei River and Kara Sea (Siberia):

785   Implications for the use of brGDGT-based proxies in coastal marine sediments, Geochim. Cosmochim.

786   Ac., 165, 200-225, https://doi.org/10.1016/j.gca.2015.05.044, 2015.

787   Doi, T., Tozuka, T., and Yamagata, T.: Interannual variability of the Guinea Dome and its

788   possible link with the Atlantic Meridional Mode, Clim. Dynam., 33, 985-998,

789   https://doi.org/10.1007/s00382-009-0574-z, 2009.

790   Duce, R. A., Liss, P. S., Merrill, J. T., Atlas, E. L Buat-Menard, P., Hicks, B. B., Miller, J. M.,

791   Prospero, J. M., Arimoto, R., Church, T. M., Ellis, W., Galloway, J. N., Hansen, L., Jickells, T. D.,

792   Knap, A. H., Reinhardt, K. H., Schneider, B., Soudine, A., Tokos, J. J., Tsunogai, S., Wollast, R., and

793   Zhou, M.: The Atmospheric Input of Trace Species to the World Ocean, Global Biogeochem. Cy., 5,

794   193-259, https://doi.org/10.1029/91gb01778, 1991.

795   Fallet, U., Brummer, G. J., Zinke, J., Vogels, S., and Ridderinkhof, H.: Contrasting seasonal

796   fluxes of planktonic foraminifera and impacts on paleothermometry in the Mozambique Channel

797   upstream of the Agulhas Current, Paleoceanography, 25, 12, https://doi.org/10.1029/2010pa001942,

798   2010.

799   Fallet, U., Ullgren, J. E., Castaneda, I. S., van Aken, H. M., Schouten, S., Ridderinkhof, H., and

800   Brummer, G. J. A.: Contrasting variability in foraminiferal and organic paleotemperature proxies in

801   sedimenting particles of the Mozambique Channel (SW Indian Ocean), Geochim. Cosmochim. Ac., 75,

802   5834-5848, https://doi.org/10.1016/j.gca.2011.08.009, 2011.

803   Fallet, U., Castaneda, I. S., Aneurin, H. E., Richter, T. O., Boer, W., Schouten, S., and Brummer,

804   G. J.: Sedimentation and burial of organic and inorganic temperature proxies in the Mozambique

805   Channel, SW Indian Ocean, Deep-Sea Res. Pt. I, 59, 37-53, https://doi.org/10.1016/j.dsr.2011.10.002,

806   2012.

807   Ferreira, A. M., Miranda, A., Caetano, M., Baas, M., Vale, C., and Sinninghe Damsté, J. S.:

808   Formation of mid-chain alkane keto-ols by post-depositional oxidation of mid-chain diols in

809   Mediterranean sapropels, Org. Geochem., 32, 271-276, https://doi.org/10.1016/S0146-6380(00)00181-

810   9, 2001.

811   Frouin, R., Franz, B. A., Werdell, P. J.: The SeaWiFS PAR product., In: S.B. Hooker and E.R.

812   Firestone, Algorithm Updates for the Fourth SeaWiFS Data Reprocessing, NASA Tech. Memo. 2003–

813   206892, Volume 22, NASA Goddard Space Flight Center, Greenbelt, Maryland, 46-50. The SeaWiFS

814   PAR product, 2003.

815   Gibbons, J. D. & Chakraborty, S.: Nonparametric Statistical Inference. Fourth Edition. Marcel

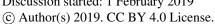816   Dekker Inc., New York, 645 pp. ISBN: 0-8247-4052-1, 2003.

817   Goddard Earth Sciences Data and Information Services Center, TRMM (TMPA-RT) Near Real-
818 Time Precipitation L3 1 day 0.25 degree x 0.25 degree V7, Greenbelt, MD, Goddard Earth Sciences
819 Data and Information Services Center (GES DISC),
820 http://disc.gsfc.nasa.gov/datacollection/TRMM_3B42RT_Daily_7.html, 2016.

821   Goñi, M. A., Woodworth, M. P., Aceves, H. L., Thunell, R. C., Tappa, E., Black, D., Müller-
822 Karger, F., Astor, Y., and Varela, R.: Generation, transport, and preservation of the alkenone-based U^K_{37}
823 sea surface temperature index in the water column and sediments of the Cariaco Basin (Venezuela),
824 Global Biogeochem. Cy., 18, 1-21, https://doi.org/10.1029/2003GB002132, 2004.

825   Gordon, A. L.: Inter-ocean exchange of thermocline water, J. Geophys. Res-Oceans, 91, 5037-
826 5046, https://doi.org/10.1029/JC091iC04p05037, 1986.

827   Goudie, A. S., and Middleton, N. J.: Saharan dust storms: nature and consequences, Earth-Sci.
828 Rev., 56, 179-204, https://doi.org/10.1016/S0012-8252(01)00067-8, 2001.

829   Guerreiro, C. V., Baumann, K. H., Brummer, G. J. A., Fischer, G., Korte, L. F., Merkel, U., Sa,
830 C., de Stigter, H., and Stuut, J. B. W.: Coccolithophore fluxes in the open tropical North Atlantic:
831 influence of thermocline depth, Amazon water, and Saharan dust, Biogeosciences, 14, 4577-4599,
832 https://doi.org/10.5194/bg-14-4577-2017, 2017.

833   Guerreiro, C. V., Baumann, K.-H., Brummer, G.-J. A., Fischer, G., Korte, L. F., Sá, C. and
834 Stuut, J.-B. W.: Wind-forced transatlantic gradients in coccolithophore species fluxes, Submitted to
835 Prog. Oceanogr. (in revision), 2018.

836   Harlander, U., Ridderinkhof, H., Schouten, M. W., and de Ruijter, W. P. M.: Long-term
837 observations of transport, eddies, and Rossby waves in the Mozambique Channel, J. Geophys. Res-
838 Oceans, 114, https://doi.org/10.1029/2008jc004846, 2009.

839   Hartnett, H. E., Keil, R. G., Hedges, J. I., and Devol, A. H.: Influence of oxygen exposure time
840 on organic carbon preservation in continental margin sediments, Nature, 391,
841 https://doi.org/10.1038/35351 572-574, 1998.

842   Hedges, J. I., Sheng Hu, F., Devol, A. H., Hartnett, H. E., Tsamakis, E., and Keil, R. G.:
843 Sedimentary organic matter preservation: a test for selective degradation under oxic conditions, Am. J.
844 Sci., 299, 529-555, https://doi.org/10.2475/ajs.299.7-9.529 1999.

845   Herndl, G. J., Reinthaler, T., Teira, E., van Aken, H., Veth, C., Pernthaler, A., and Pernthaler,
846 J.: Contribution of *Archaea* to total prokaryotic production in the deep Atlantic Ocean, Appl. Environ.
847 Microb., 71, 2303-2309, https://doi.org/10.1128/aem.71.5.2303-2309.2005, 2005.

848   Honjo, S., and Doherty, K. W.: Large aperture time-series sediment traps; design objectives,
849   construction and application, Deep Sea Res., 35, 133-149, https://doi.org/10.1016/0198-
850   0149(88)90062-3, 1988.

851   Hopmans, E. C., Weijers, J. W. H., Schefuß, E., Herfort, L., Sinninghe Damsté, J. S., and
852   Schouten, S.: A novel proxy for terrestrial organic matter in sediments based on branched and isoprenoid
853   tetraether lipids, Earth Planet. Sc. Lett., 224, 107-116, https://doi.org/10.1016/j.epsl.2004.05.012, 2004.

854   Hopmans, E. C., Schouten, S., and Sinninghe Damsté, J. S.: The effect of improved
855   chromatography on GDGT-based palaeoproxies, Org. Geochem., 93, 1-6,
856   http://dx.doi.org/10.1016/j.orggeochem.2015.12.006, 2016.

857   Huffman, G.J., Adler, R.F., Bolvin, D.T., Gu, G., Nelkin, E.J., Bowman, K.P., Hong, Y.,
858   Stocker, E.F., Wolff, D.B.: The TRMM Multi-satellite Precipitation Analysis: Quasi- Global, Multi-
859   Year, Combined-Sensor Precipitation Estimates at Fine Scale. J. Hydrometeor. 8 (1), 38-55,
860   https://doi.org/10.1175/JHM560.1, 2007.

861   Hughen, K. A., Overpeck, J. T., Peterson, L. C., and Anderson, R. F.: The nature of varved
862   sedimentation in the Cariaco Basin, Venezuela, and its palaeoclimatic significance, Geological Society,
863   London, Special Publications, 116, 171-183, https://doi.org/10.1144/gsl.Sp.1996.116.01.15, 1996.

864   Hughen, K. A., Overpeck, J. T., Lehman, S. J., Kashgarian, M., Southon, J., Peterson, L. C.,
865   Alley, R., and Sigman, D. M.: Deglacial changes in ocean circulation from an extended radiocarbon
866   calibration, Nature, 391, 65-68, https://doi.org/10.1038/34150, 1998.

867   Huguet, C., Hopmans, E. C., Febo-Ayala, W., Thompson, D. H., Sinninghe Damsté, J. S., and
868   Schouten, S.: An improved method to determine the absolute abundance of glycerol dibiphytanyl
869   glycerol tetraether lipids, Org. Geochem., 37, 1036-1041,
870   https://doi.org/10.1016/j.orggeochem.2006.05.0082006.

871   Huguet, C., Schimmelmann, A., Thunell, R., Lourens, L. J., Sinninghe Damsté, J. S., and
872   Schouten, S.: A study of the TEX$_{86}$ paleothermometer in the water column and sediments of the Santa
873   Barbara Basin, California, Paleoceanography, 22, https://doi.org/10.1029/2006pa001310, 2007.

874   Jiang, S., O'Leary, T., Volkman, J. K., Zhang, H., Jia, R., Yu, S., Wang, Y., Luan, Z., Sun, Z.,
875   and Jiang, R.: Origins and simulated thermal alteration of sterols and keto-alcohols in deep-sea marine-
876   sediments of the Okinawa Trough, Org. Geochem., 21, 415-422, https://doi.org/10.1016/0146-
877   6380(94)90203-8, 1994.

878   Jonas, A. S., Schwark, L., and Bauersachs, T.: Late Quaternary water temperature variations of
879   the Northwest Pacific based on the lipid paleothermometers TEX$_{86}$^{H}, U$^{K'}_{37}$ and LDI, Deep-Sea Res. Pt.
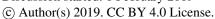880   I, 125, 81-93, http://doi.org/10.1016/j.dsr.2017.04.018, 2017.

881   Karner, M. B., DeLong, E. F., and Karl, D. M.: Archaeal dominance in the mesopelagic zone
882   of the Pacific Ocean, Nature, 409, 507-510, https://doi.org/10.1038/35054051, 2001.

883   Kim, J.-H., Schouten, S., Hopmans, E. C., Donner, B., and Sinninghe Damsté, J. S.: Global
884   sediment core-top calibration of the TEX$_{86}$ paleothermometer in the ocean, Geochim. Cosmochim. Ac.,
885   72, 1154-1173, https://doi.org/10.1016/j.gca.2007.12.010, 2008.

886   Kim, J.-H., van der Meer, J., Schouten, S., Helmke, P., Willmott, V., Sangiorgi, F., Koc, N.,
887   Hopmans, E. C., and Sinninghe Damsté, J. S.: New indices and calibrations derived from the distribution
888   of crenarchaeal isoprenoid tetraether lipids: Implications for past sea surface temperature
889   reconstructions, Geochim. Cosmochim. Ac., 74, 4639-4654, https://doi.org/10.1016/j.gca.2010.05.027,
890   2010.

891   Kim, J.-H., Romero, O. E., Lohmann, G., Donner, B., Laepple, T., Haam, E., and Sinninghe
892   Damsté, J. S.: Pronounced subsurface cooling of North Atlantic waters off Northwest Africa during
893   Dansgaard–Oeschger   interstadials,   Earth   Planet.   Sc.   Lett.,   339-340,   95-102,
894   https://doi.org/10.1016/j.epsl.2012.05.018, 2012.

895   Kim, J.-H., Schouten, S., Rodrigo-Gámiz, M., Rampen, S., Marino, G., Huguet, C., Helmke, P.,
896   Buscail, R., Hopmans, E. C., Pross, J., Sangiorgi, F., Middelburg, J. B. M., and Sinninghe Damsté, J.
897   S.: Influence of deep-water derived isoprenoid tetraether lipids on the TEX$_{86}^{H}$ paleothermometer in the
898   Mediterranean   Sea,   Geochim.   Cosmochim.   Ac.,   150,   125-141,
899   https://doi.org/10.1016/j.gca.2014.11.017, 2015.

900   Koning, E., van Iperen, J. M., van Raaphorst, W., Helder, W., Brummer, G.-J. A., and van
901   Weering, T. C. E.: Selective preservation of upwelling-indicating diatoms in sediments off Somalia,
902   NW Indian Ocean, Deep-Sea Res. Pt. I, 48, 2473-2495, https://doi.org/10.1016/S0967-0637(01)00019-
903   X, 2001.

904   Korte, L. F., Brummer, G. J. A., van der Does, M., Guerreiro, C. V., Hennekam, R., van Hateren,
905   J. A., Jong, D., Munday, C. I., Schouten, S., and Stuut, J. B. W.: Downward particle fluxes of biogenic
906   matter and Saharan dust across the equatorial North Atlantic, Atmos. Chem. Phys., 17, 6023-6040,
907   https://doi.org/10.5194/acp-17-6023-2017, 2017.

908   Lange, C. B., Romero, O. E., Wefer, G., and Gabric, A. J.: Offshore influence of coastal
909   upwelling off Mauritania, NW Africa, as recorded by diatoms in sediment traps at 2195 m water depth,
910   Deep-Sea Res. Pt. I, 45, 986-1013, https://doi.org/10.1016/s0967-0637(97)00103-9 1998.

911   Lattaud, J., Kim, J.-H., De Jonge, C., Zell, C., Sinninghe Damsté, J. S., and Schouten, S.: The
912   C$_{32}$ alkane-1,15-diol as a tracer for riverine input in coastal seas, Geochim. Cosmochim. Ac., 202, 146-
913   158, http://doi.org/10.1016/j.gca.2016.12.030, 2017a.

914   Lattaud, J., Dorhout, D., Schulz, H., Castañeda, I. S., Schefuß, E., Sinninghe Damsté, J. S., and

915   Schouten, S.: The C$_{32}$ alkane-1,15-diol as a proxy of late Quaternary riverine input in coastal margins,

916   Clim. Past, 13, 1049-1061, http://doi.org/10.5194/cp-13-1049-2017, 2017b.

917   Lee, T., Lagerloef, G., Gierach, M.M., Kao, H.-Y., Yueh, S., Dohan, K.: Aquarius reveals

918   salinity   structure   of   tropical   instability   waves,   Geophys.   Res.   Lett.,   39,   L12610,

919   https://doi.org/10.1029/2012GL052232, 2012.

920   Lefèvre, N., Moore, G., Aiken, J., Watson, A., and Cooper, D.: Variability of pCO2 in the

921   tropical Atlantic in 1995, J. Geophys. Res., C3, 5623-5634, https://doi.org/10.1029/97JC023031998.

922   Ljung, G. M., & Box, G. E.: On a measure of lack of fit in time series models. Biometrika,

923   65(2), 297-303, https://www.jstor.org/stable/2335207, 1978.

924   Locarnini R. A., Mishonov A. V., Antonov J. I., Boyer T. P., Garcia H. E., Baranova O. K.,

925   Zweng M. M., Paver C. R., Reagan J. R., Johnson D. R., Hamilton M., Seidov D.: World Ocean Atlas

926   2013, Volume 1: temperature. Levitus S, Ed.; Mishonov A, Technical Ed.; NOAA Atlas NESDIS 73,

927   40 pp, 2013.

928   Lopes dos Santos, R. A., Prange, M., Castañeda, I. S., Schefuß, E., Mulitza, S., Schulz, M.,

929   Niedermeyer, E. M., Sinninghe Damsté, J. S., and Schouten, S.: Glacial-interglacial variability in

930   Atlantic meridional overturning circulation and thermocline adjustments in the tropical North Atlantic,

931   Earth Planet. Sc. Lett., 300, 407-414, https://doi.org/10.1016/j.epsl.2010.10.030, 2010.

932   Lopes dos Santos, R. A. L., Spooner, M. I., Barrows, T. T., De Deckker, P., Sinninghe Damsté,

933   J. S., and Schouten, S.: Comparison of organic (U$^{K'}_{37}$, TEX$_{86}^{H}$, LDI) and faunal proxies (foraminiferal

934   assemblages) for reconstruction of late Quaternary sea surface temperature variability from offshore

935   southeastern Australia, Paleoceanography, 28, 377-387, https://doi.org/10.1002/palo.20035, 2013.

936   Lutjeharms, J. R. E.: The Agulhas Current, 330 pp., Springer, Berlin, 2006.

937   Malauene, B. S., Shillington, F. A., Roberts, M. J., and Moloney, C. L.: Cool, elevated

938   chlorophyll-a   waters   off   northern   Mozambique,   Deep-Sea   Res.   Pt.   II,   100,   68-78,

939   https://doi.org/10.1016/j.dsr2.2013.10.017, 2014.

940   Marlowe, I. T., Green, J. C., Neal, A. C., Brassell, S. C., Eglinton, G., and Course, P. A.: Long-

941   Chain (n-C$_{37}$–C$_{39}$) alkenones in the Prymnesiophyceae. Distribution of alkenones and other lipids and

942   their   taxonomic   significance,   Brit.   Phycol.   J.,   19,   203-216,

943   https://doi.org/10.1080/00071618400650221, 1984.

944   Martin, J. H., and Fitzwater, S. E.: Iron-deficiency limits phytoplankton growth in the Northeast

945   Pacific Subarctic, Nature, 331, 341-343, https://doi.org/10.1038/331341a0, 1988.

946   Mazeika, P. A.: Thermal domes in the Eastern Tropical Atlantic Ocean. Limnol. Oceanogr., 12,
947   537-539, https://doi.org/10.4319/lo.1967.12.3.0537, 1967.

948   Méjanelle, L., Sanchez-Gargallo, A., Bentaleb, I., and Grimalt, J. O.: Long chain *n*-alkyl diols,
949   hydroxy ketones and sterols in a marine eustigmatophyte, *Nannochloropsis gaditana*, and in *Brachionus*
950   *plicatilis* feeding on the algae, Org. Geochem., 34, 527-538, Pii s0146-6380(02)00246-2,
951   https://doi.org/10.1016/s0146-6380(02)00246-2, 2003.

952   Müller-Karger, F. E., McClain, C. R., and Richardson, P. L.: The dispersal of the Amazon´s
953   water, Nature, 333, 56-59, https://doi.org/10.1038/333056a0 1988.

954   Müller-Karger, F. E., Richardson, P. L., and McGillicuddy, D.: On the offshore dispersal of the
955   Amazon´s Plume in the North Atlantic: Comments on the paper by A. Longhurst, "Seasonal cooling and
956   blooming in tropical oceans", Deep-Sea Res. Pt. I, 42, 2127-2137, https://doi.org/10.1016/0967-
957   0637(95)00085-2, 1995.

958   Müller-Karger, F., Varela, R., Thunell, R., Scranton, M., Bohrer, R., Taylor, G., Capelo, J.,
959   Astor, Y., Tappa, E., Ho, T. Y., and Walsh, J. J.: Annual cycle of primary production in the Cariaco
960   Basin: Response to upwelling and implications for vertical export, J. Geophys. Res., 106, 4527-4542,
961   https://doi.org/10.1029/1999JC000291, 2001.

962   Müller-Karger, F., Varela, R., Thunell, R., Astor, Y., Zhang, H. Y., Luerssen, R., and Hu, C.
963   M.: Processes of coastal upwelling and carbon flux in the Cariaco Basin, Deep-Sea Res. Pt. II, 51, 927-
964   943, https://doi.org/10.1016/j.dsr2.2003.10.010, 2004.

965   Müller, P. J., Kirst, G., Ruhland, G., von Storch, I., and Rosell-Melé, A.: Calibration of the
966   alkenone paleotemperature index U^{K}_{37} based on core-tops from the eastern South Atlantic and the global
967   ocean (60°N-60°S), Geochim. Cosmochim. Ac., 62, 1757-1772, https://doi.org/10.1016/s0016-
968   7037(98)00097-0, 1998.

969   Müller, P. J., and Fischer, G.: A 4-year sediment trap record of alkenones from the filamentous
970   upwelling region off Cape Blanc, NW Africa and a comparison with distributions in underlying
971   sediments, Deep-Sea Res. Pt. I, 48, 1877-1903, https://doi.org/10.1016/S0967-0637(00)00109-6, 2001.

972   Naafs, B. D. A., Hefter, J., and Stein, R.: Application of the long chain diol index (LDI)
973   paleothermometer to the early Pleistocene (MIS 96), Org. Geochem., 49, 83-85,
974   http://doi.org/10.1016/j.orggeochem.2012.05.011, 2012.

975   NASA Aquarius project: Aquarius Official Release Level 3 Sea Surface Salinity Standard
976   Mapped Image Daily Data V4.0. Ver. 4.0. PO.DAAC, CA, USA, 2015a.

977   NASA Aquarius project: Aquarius Official Release Level 3 Wind Speed Standard Mapped
978   Image Daily Data V4.0. Ver. 4.0. PO.DAAC, CA, USA, 2015b.

979   Nehring, D., Hagen, E., Jorge da Silva, A., Schemainda, R., Wolf, G., Michelchen, N., Kaiser,
980   W., Postel, L., Gosselk, F., and Brenning, U.: The oceanological conditions in the western part of the
981   Mozambique Channel in February-March 1980, 1984.

982   Peeters, F. J. C., Acheson, R., Brummer, G. J. A., de Ruijter, W. P. M., Schneider, R. R.,
983   Ganssen, G. M., Ufkes, E., and Kroon, D.: Vigorous exchange between the Indian and Atlantic oceans
984   at the end of the past five glacial periods, Nature, 430, 661-665, http://doi.org/10.1038/nature02785,
985   2004.

986   Peterson, L. C., Overpeck, J. T., Kipp, N. G., and Imbrie, J.: A high-resolution Late Quaternary
987   upwelling record from the anoxic Cariaco Basin, Venezuela, Paleoceanography, 6, 99-119,
988   http://doi.org/10.1029/90pa02497, 1991.

989   Prahl, F. G., and Wakeham, S. G.: Calibration of unsaturation patterns in long-chain ketone
990   compositions for paleotemperature assessment, Nature, 330, 367-369, http://doi.org/10.1038/330367a0,
991   1987.

992   Prahl, F. G., Dymond, J., and Sparrow, M. A.: Annual biomarker record for export production
993   in the central Arabian Sea, Deep-Sea Res. II, 47, 1581-1604, https://doi.org/10.1016/S0967-
994   0645(99)00155-1, 2000.

995   Rampen, S. W., Schouten, S., Wakeham, S. G., and Sinninghe Damsté, J. S.: Seasonal and
996   spatial variation in the sources and fluxes of long chain diols and mid-chain hydroxy methyl alkanoates
997   in the Arabian Sea, Org. Geochem., 38, 165-179, https://doi.org/10.1016/j.orggepchem.2006.10.008,
998   2007.

999   Rampen, S. W., Schouten, S., Koning, E., Brummer, G.-J. A., and Sinninghe Damsté, J. S.: A
1000   90 kyr upwelling record from the northwestern Indian Ocean using a novel long-chain diol index, Earth
1001   Planet. Sc. Lett., 276, 207-213, https://doi.org/10.1016/j.epsl.2008.09.0222008.

1002   Rampen, S. W., Schouten, S., and Sinninghe Damsté, J. S.: Occurrence of long chain 1,14-diols
1003   in *Apedinella radians*, Org. Geochem., 42, 572-574, https://doi.org/10.1016/j.orggeochem.2011.03.009,
1004   2011.

1005   Rampen, S. W., Willmott, V., Kim, J. H., Uliana, E., Mollenhauer, G., Schefuss, E., Sinninghe
1006   Damsté, J. S., and Schouten, S.: Long chain 1,13-and 1,15-diols as a potential proxy for
1007   palaeotemperature   reconstruction,   Geochim.   Cosmochim.   Ac.,   84,   204-216,
1008   https://doi.org/10.1016/j.gca.2012.01.024, 2012.

1009   Rampen, S. W., Willmott, V., Kim, J. H., Rodrigo-Gámiz, M., Uliana, E., Mollenhauer, G.,
1010   Schefuss, E., Sinninghe Damsté, J. S., and Schouten, S.: Evaluation of long chain 1,14-alkyl diols in
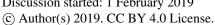
1011   marine sediments as indicators for upwelling and temperature, Org. Geochem., 76, 39-47,

1012   https://doi.org/10.1016/j.orggeochem.2014.07.012, 2014a.

1013   Rampen, S. W., Datema, M., Rodrigo-Gámiz, M., Schouten, S., Reichart, G. J., and Sinninghe

1014   Damsté, J. S.: Sources and proxy potential of long chain alkyl diols in lacustrine environments,

1015   Geochim. Cosmochim. Ac., 144, 59-71, https://doi.org/10.1016/j.gca.2014.08.033, 2014b.

1016   Reiche, S., Rampen, S. W., Dorhout, D. J. C., Sinninghe Damsté, J. S., and Schouten, S.: The

1017   impact of oxygen exposure on long-chain alkyl diols and the long chain diol index (LDI) – a long-term

1018   incubation study, Org. Geochem., 124, 238-246, https://doi.org/10.1016/j.orggeochem.2018.08.003,

1019   2018.

1020   Richards, F. A. 1975. The Cariaco Basin (Trench). Oceanogr. Mar. Biol. Ann. Rev. 13: 11–67.

1021   Richardson, P. L., and Reverdin, G.: Seasonal cycle of velocity in the Atlantic North Equatorial

1022   Countercurrent as measured by surface drifters, current meters, and ship drifts, J. Geophys. Res.-Oceans,

1023   92, 3691-3708, https://doi.org/10.1029/JC092iC04p03691, 1987.

1024   Ridderinkhof, H., van der Werf, P. M., Ullgren, J. E., van Aken, H. M., van Leeuwen, P. J., and

1025   de Ruijter, W. P. M.: Seasonal and interannual variability in the Mozambique Channel from moored

1026   current observations, J. Geophys. Res.-Oceans, 115, https://doi.org/10.1029/2009jc005619, 2010.

1027   Rodrigo-Gámiz, M., Rampen, S. W., de Haas, H., Baas, M., Schouten, S., and Sinninghe

1028   Damsté, J. S.: Constraints on the applicability of the organic temperature proxies $U^{K'}_{37}$, TEX_{86} and LDI

1029   in the subpolar region around Iceland, Biogeosciences, 12, 6573-6590, https://doi.org/10.5194/bg-12-

1030   6573-2015, 2015.

1031   Rodrigo-Gámiz, M., Rampen, S. W., Schouten, S., and Sinninghe Damsté, J. S.: The impact of

1032   oxic degradation on long chain alkyl diol distributions in Arabian Sea surface sediments, Org.

1033   Geochem., 100, 1-9, http://doi.org/10.1016/j.orggeochem.2016.07.003, 2016.

1034   Romero O. E., Lange C. B., Fischer G., Treppke U. F., Wefer G.: Variability in Export

1035   Production Documented by Downward Fluxes and Species Composition of Marine Planktic Diatoms:

1036   Observations from the Tropical and Equatorial Atlantic. In: Fischer G., Wefer G. (eds) Use of Proxies

1037   in Paleoceanography. Springer, Berlin, Heidelberg, 1999.

1038   Rosell-Melé, A., and Prahl, F. G.: Seasonality of $U^{K'}_{37}$ temperature estimates as inferred from

1039   sediment trap data, Quaternary Sci. Rev., 72, 128-136, https://doi.org/10.1016/j.quascirev.2013.04.017,

1040   2013.

1041   Rossignol, M., and A.M. Meyruis, Campagnes océanographiques du Gérard-Tréca, 53 pp.,

1042   Cent. Oceanogr. Dakar-Thiaroye, ORSTOM, Dakar, Senegal, 1964.

1043   Sætre, R., and Da Silva, A. J.: The circulation of the Mozambique channel, Deep Sea Res., 31,

1044   485-508, https://doi.org/10.1016/0198-0149(84)90098-0, 1984.

1045   Schlitzer, R.: Data Analysis and Visualization with Ocean Data View, CMOS Bulletin SCMO,

1046   43, 9–13, available at: https://odv.awi.de/, 2015.

1047   Schouten, M. W., de Ruijter, W. P. M., van Leeuwen, P. J., and Ridderinkhof, H.: Eddies and

1048   variability in the Mozambique Channel, Deep-Sea Res. Pt. II, 50, 1987-2003,

1049   https://doi.org/10.1016/s0967-0645(03)00042-0, 2003.

1050   Schouten, S., Hopmans, E. C., Schefuss, E., and Sinninghe Damsté, J. S.: Distributional

1051   variations in marine crenarchaeotal membrane lipids: a new tool for reconstructing ancient sea water

1052   temperatures?, Earth Planet. Sc. Lett., 204, 265-274, https://doi.org/10.1016/s0012-821x(02)00979-2,

1053   2002.

1054   Schouten, S., Hopmans, E. C., and Sinninghe Damsté, J. S.: The organic geochemistry of

1055   glycerol dialkyl glycerol tetraether lipids: A review, Org. Geochem., 54, 19-61,

1056   https://doi.org/10.1016/j.orggeochem.2012.09.006, 2013.

1057   Schreuder, L. T., Stuut, J.-B. W., Korte, L. F., Sinninghe Damsté, J. S., and Schouten, S.:

1058   Aeolian transport and deposition of plant wax *n*-alkanes across the tropical North Atlantic Ocean, Org.

1059   Geochem., 115, 113-123, https://doi.org/10.1016/j.orggeochem.2017.10.010, 2018a.

1060   Schreuder, L. T., Hopmans, E. C., Stuut, J.-B. W., Sinninghe Damsté, J. S., and Schouten, S.:

1061   Transport and deposition of the fire biomarker levoglucosan across the tropical North Atlantic Ocean,

1062   Geochim. Cosmochim. Ac., 227, 171-185, https://doi.org/10.1016/j.gca.2018.02.020, 2018b.

1063   Siedler, G., Zangenberg, N., and Onken, R.: Seasonal Changes in the Tropical Atlantic

1064   Circulation – Observation and Simulation of the Guinea Dome, J. Geophys. Res.-Oceans, 97, 703-715,

1065   https://doi.org/10.1029/91jc02501, 1992.

1066   Sinninghe Damsté, J. S., Rijpstra, W. I. C., Hopmans, E. C., Prahl, F. G., Wakeham, S. G., and

1067   Schouten, S.: Distribution of membrane lipids of planktonic Crenarchaeota in the Arabian seat, App.

1068   Environ. Micr., 68, 2997-3002, https://doi.org/10.1128/aem.68.6.2997-3002.2002, 2002.

1069   Sinninghe Damsté, J. S., Rijpstra, W. I. C., and Reichart, G.-J.: The influence of oxic

1070   degradation on the sedimentary biomarker record II. Evidence from Arabian Sea sediments, Geochim.

1071   Cosmochim. Ac., 66, 2737-2754, https://doi.org/10.1016/S0016-7037(02)00865-7, 2002.

1072   Sinninghe Damsté, J. S., Rampen, S., Rijpstra, W. I. C., Abbas, B., Muyzer, G., and Schouten,

1073   S.: A diatomaceous origin for long-chain diols and mid-chain hydroxy methyl alkanoates widely

1074   occurring in Quaternary marine sediments: Indicators for high-nutrient conditions, Geochim.

1075   Cosmochim. Ac., 67, 1339-1348, https://doi.org/10.1016/s0016-7037(02)01225-5 2003.

1076   Sinninghe Damsté, J. S., Rijpstra, W. I. C., Hopmans, E. C., den Uijl, M. J., Weijers, J. W. H.,
1077   and Schouten, S.: The enigmatic structure of the crenarchaeol isomer, Org. Geochem., 124, 22-28,
1078   https://doi.org/10.1016/j.orggeochem.2018.06.005, 2018.

1079   Smith, S. L.: Understanding the Arabian Sea: Reflections on the 1994-1996 Arabian Sea
1080   Expedition, Deep-Sea Res. Pt. II, 48, 1385-1402, https://doi.org/10.1016/S0967-0645(00)00144-2,
1081   2001.

1082   Stramma, L., and Schott, F.: The mean flow field of the tropical Atlantic Ocean, Deep-Sea Res.
1083   Pt. II, 46, 279-303, https://doi.org/10.1016/s0967-0645(98)00109-x, 1999.

1084   Stuut, J.-B., Zabel, M., Ratmeyer, V., Helmke, P., Schefuß, E., Lavik, G., and Schneider, R.:
1085   Provenance of present-day eolian dust collected off NW Africa, J. .Geophys. Res.-Atmos., 110, D04202-
1086   04201-D04202-04214, https://doi.org/10.1029/2004JD005161, 2005.

1087   Thunell, R. C., Varela, R., Llano, M., Collister, J., Müller-Karger, F., and Bohrer, R.: Organic
1088   carbon fluxes, degradation, and accumulation in an anoxic basin: Sediment trap results from the Cariaco
1089   Basin, Limnol. Oceanogr., 45, 300-308, https://doi.org/10.4319/lo.2000.45.2.0300, 2000.

1090   Thunell, R., Benitez-Nelson, C., Varela, R., Astor, Y., and Müller-Karger, F.: Particulate
1091   organic carbon fluxes along upwelling-dominated continental margins: Rates and mechanisms, Global
1092   Biogeochem. Cy., 21, https://doi.org/10.1029/2006gb002793, 2007.

1093   Tierney, J. E., and Tingley, M. P.: A Bayesian, spatially-varying calibration model for the TEX_{86}
1094   proxy, Geochim. Cosmochim. Ac., 127, 83-106, https://doi.org/10.1016/j.gca.2013.11.026, 2014.

1095   Tierney, J. E., and Tingley, M. P.: A TEX_{86} surface sediment database and extended Bayesian
1096   calibration, Scientific Data, 2, 150029, https://doi.org/10.1038/sdata.2015.29, 2015.

1097   Tierney, J. E., Sinninghe Damsté, J. S., Pancost, R. D., Sluijs, A., and Zachos, J. C.: Eocene
1098   temperature gradients, Nature Geosci, 10, 538-539, https://doi.org/10.1038/ngeo2997, 2017

1099   Tierney, J. E., and Tingley, M. P.: BAYSPLINE: A New Calibration for the Alkenone
1100   Paleothermometer,   Paleoceanography   and   Paleoclimatology,   33,   281-301,
1101   https://doi.org/10.1002/2017pa003201, 2018.

1102   Torrence, C., Compo, G. P.: A practical guide to wavelet analysis. Bull. Am. Meteorol. Soc.79,
1103   61–78, https://doi.org/10.1175/1520-0477(1998)079<0061:APGTWA>2.0.CO;2, 1998.

1104   Treppke, U. F., Lange, C. B., and Wefer, G.: Vertical fluxes of diatoms and silicoflagellates in
1105   the eastern equatorial Atlantic, and their contribution to the sedimentary record, Mar. Micropaleontol.,
1106   28, 73-96, https://doi.org/10.1016/0377-8398(95)00046-1, 1996.

1107   Turich, C., Schouten, S., Thunell, R. C., Varela, R., Astor, Y., and Wakeham, S. G.: Comparison

1108 of TEX$_{86}$ and U$^{K'}_{37}$ temperature proxies in sinking particles in the Cariaco Basin, Deep-Sea Res. Pt. I,

1109 78, 115-133, http://doi.org/10.1016/j.dsr.2013.02.008, 2013.

1110   Ullgren, J. E., van Aken, H. M., Ridderinkhof, H. and de Ruijter, W. P. M.: The hydrography

1111 of the Mozambique Channel from six years of continuous temperature, salinity, and velocity

1112 observations. Deep-Sea Res. Pt. I, 69, 36 – 50, https://doi.org/10.1016/j.dsr.2012.07.003, 2012.

1113   Villanueva, L., Besseling, M., Rodrigo-Gámiz, M., Rampen, S. W., Verschuren, D., and

1114 Sinninghe Damsté, J. S.: Potential biological sources of long chain alkyl diols in a lacustrine system,

1115 Org. Geochem., 68, 27-30, https://doi.org/10.1016/j.orggeochem.2014.01.001, 2014.

1116   van der Does, M., Korte, L. F., Munday, C. I., Brummer, G. J. A., and Stuut, J. B. W.: Particle

1117 size traces modern Saharan dust transport and deposition across the equatorial North Atlantic, Atmos.

1118 Chemis. Phys., 16, 13697-13710, https://doi.org/10.5194/acp-16-13697-2016, 2016.

1119   Versteegh, G. J. M., Bosch, H. J., and de Leeuw, J. W.: Potential palaeoenvironmental

1120 information of C$_{24}$ to C$_{36}$ mid-chain diols, keto-ols and mid-chain hydroxy fatty acids; a critical review,

1121 Org. Geochem., 27, 1-13, https://doi.org/10.1016/s0146-6380(97)00063-6, 1997.

1122   Versteegh, G. J. M., Jansen, J. H. F., de Leeuw, J. W., and Schneider, R. R.: Mid-chain diols

1123 and keto-ols in SE Atlantic sediments: a new tool for tracing past sea surface water masses?, Geochim.

1124 Cosmochim. Ac., 64, 1879-1892, https://doi.org/10.1016/S0016-7037(99)00398-1, 2000.

1125   Voituriez, B.: Les sous-courants 6quatoriaux nord et sud et la formation des dômes thermiques

1126 tropicaux, Oceanol. Acta, 4,497-506, 1981.

1127   Volkman, J. K., Eglinton, G., Corner, E. D. S., and Sargent, J. R.: Novel unsaturated straight-

1128 chain C$_{37}$-C$_{39}$ methyl and ethyl ketones in marine sediments and a coccolithophore *Emiliania huxleyi*,

1129 Phys. Chem. Earth, 12, 219-227, http://doi.org/10.1016/0079-1946(79)90106-X, 1980.

1130   Volkman, J. K., Barrett, S. M., Dunstan, G. A., and Jeffrey, S. W.: C$_{30}$–C$_{32}$ alky diols and

1131 unsaturated alcohols in microalgae of the class Eustigmatophyceae, Org. Geochem., 18, 131-138,

1132 http://doi.org/10.1016/0146-6380(92)90150-v, 1992.

1133   Volkman, J. K., Barrett, S. M., Blackburn, S. I., and Sikes, E. L.: Alkenones in *Gephyrocapsa*

1134 *Oceanica* – Implications for studies of paleoclimate, Geochim. Cosmochim. Ac., 59, 513-520,

1135 http://doi.org/10.1016/0016-7037(95)00325-t, 1995.

1136   Volkman, J. K., Barrett, S. M., and Blackburn, S. I.: Eustigmatophyte microalgae are potential

1137 sources of C$_{29}$ sterols, C$_{22}$–C$_{28}$ *n*-alcohols and C$_{28}$–C$_{32}$ *n*-alkyl diols in freshwater environments, Org.

1138 Geochem., 30, 307-318, http://doi.org/10.1016/s0146-6380(99)00009-1, 1999.

1139   Wakeham, S. G., Peterson, M. L., Hedges, J. I., and Lee, C.: Lipid biomarker fluxes in the

1140   Arabian Sea, with a comparison to the equatorial Pacific Ocean, Deep-Sea Res. Pt. II, 49, 2265-2301,

1141   https://doi.org/10.1016/S0967-0645(02)00037-1, 2002.

1142   Warnock, J. P., Bauersachs, T., Kotthoff, U., Brandt, H. T., and Andren, E.: Holocene

1143   environmental history of the Angermanalven Estuary, northern Baltic Sea, Boreas, 47, 593-608,

1144   https://doi.org/10.1111/bor.12281, 2018.

1145   Weijer, W., de Ruiter, W. P. M., Dijkstra, H. A., and van Leeuwen, P. J.: Impact of interbasin

1146   exchange on the Atlantic overturning circulation, J. Phys. Oceanogr., 29, 2266-2284,

1147   https://doi.org/10.1175/1520-0485(1999)029<2266:Ioieot>2.0.Co;2, 1999.

1148   Willmott, V., Rampen, S. W., Domack, E., Canals, M., Sinninghe Damsté, J. S., and Schouten,

1149   S.: Holocene changes in Proboscia diatom productivity in shelf waters of the north-western Antarctic

1150   Peninsula, Antarct. Sci., 22, 3-10, https://doi.org/10.1017/s095410200999037x, 2010.

1151   Wuchter, C., Schouten, S., Wakeham, S. G., and Sinninghe Damsté, J. S.: Temporal and spatial

1152   variation in tetraether membrane lipids of marine Crenarchaeota in particulate organic matter:

1153   Implications   for TEX_{86} paleothermometry,   Paleoceanography,   20,

1154   https://doi.org/10.1029/2004pa001110, 2005.

1155   Wuchter, C., Schouten, S., Wakeham, S. G., and Sinninghe Damsté, J. S.: Archaeal tetraether

1156   membrane lipid fluxes in the northeastern Pacific and the Arabian Sea: Implications for TEX_{86}

1157   paleothermometry,   Paleoceanography,   21,   PA4208-4201-PA4208-4209,

1158   https://doi.org/10.1029/2006PA001279, 2006.

1159   Xie, P. and Arkin, P.A.: Global precipitation: A 17-year monthly analysis based on gauge

1160   observations, satellite estimates, and numerical model outputs. Bull. Am. Meteor. Soc., 78, 2539 – 2558,

1161   https://doi.org/10.1175/1520-0477(1997)078<2539:GPAYMA>2.0.CO;2, 1997.

1162   Yamagata, T., and Iizuka, S.: Simulation of the Tropical Thermal Domes in the Atlantic – A

1163   Seasonal   Cycle,   J.   Phys.   Oceanogr.,   25,   2129-2140,   https://doi.org/10.1175/1520-

1164   0485(1995)025<2129:Sotttd>2.0.Co;2, 1995.

1165   Yamamoto, M., Shimamoto, A., Fukuhara, T., Tanaka, Y., and Ishizaka, J.: Glycerol dialkyl

1166   glycerol tetraethers and TEX_{86} index in sinking particles in the western North Pacific, Org. Geochem.,

1167   53, 52-62, https://doi.org/10.1016/j.orggeochem.2012.04.010, 2012.

1168   Zhang, Y. G., and Liu, X. Q.: Export Depth of the TEX_{86} Signal, Paleoceanography and

1169   Paleoclimatology, 33, 666-671, https://doi.org/10.1029/2018PA003337, 2018.
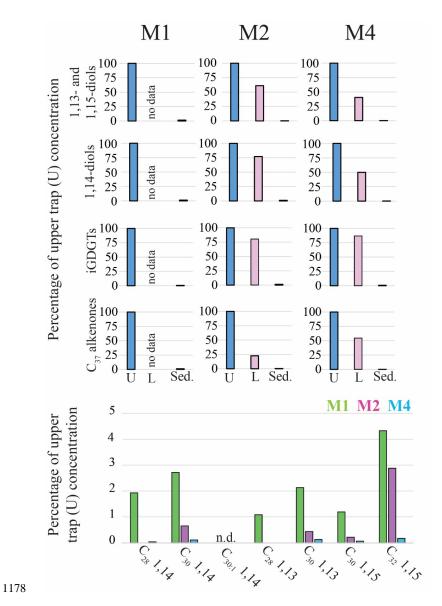
1170

1171

Fig. 1 **(a)** Location map showing the five sediment trap mooring sites in the Cariaco Basin, the tropical North Atlantic (M1, M2 and M4) and the Mozambique Channel. Two of the moorings in the tropical North Atlantic (M2 and M4) contain an upper ('U') and a lower ('L') trap, shown in the bathymetric section below **(b)** with traps depicted as red triangles and surface sediments shown as black crosses. A similar section profile is shown for the Mozambique Channel (c), where also the sediment trap and the surface sediments are indicated. All maps/sections are generated in Ocean Data View (Schlitzer, 2015).

1178

Fig. 2 Relative concentrations of biomarker lipids for the mooring sites M1, M2 and M4 in the tropical

North Atlantic. Upper panel: percentages of lipid biomarkers in the lower traps ('L'; 3500 m) and the

surface sediments ('Sed.') relative to the annual flux-weighted concentrations in the upper traps ('U';

1200 m; set at 100%). The lower panel shows the preservation of the individual LCDs (sediments versus

upper trap flux-weighted concentration) for the three sediment trap sites. For M1 and M2 the

sedimentary LCD concentration were based on the average of the two nearby underlying surface

sediments (Fig. 1). When no bar is shown than the LCD was not detected.

1186

Fig. 3 Lipid biomarker fluxes for the tropical North Atlantic sediment traps, i.e., M1, upper and lower M2, and upper and lower M4 in panels **(a)** to **(e)**. Lipid biomarker fluxes (iGDGTs in purple; C_{37} alkenones in orange; 1,13- and 1,15-diols in black; 1,14-diols in red) are indicated on the left *y*-axis, and the total mass flux (grey stack; Korte et al., 2017) on the right *y*-axis. Lipid biomarker concentrations are plotted in panels **(f)** to **(j)**, with biomarker concentrations on the left *y*-axis, and the total mass flux on the right *y*-axis. Note that the *y*-axes are different per sediment trap site, but identical for upper (U) and lower (L) traps.

45

1196

Fig. 4 Seasonal summed flux-weighted average of 1,13-/1,15-diol concentrations in all sediment traps
(station M1 upper trap, station M2 upper and lower trap and station M4 upper and lower trap) of the
tropical North Atlantic.

1197
1198
1199

1200

1201

Fig. 5 Temperature proxy records for the tropical North Atlantic. Panel **(a)** shows upper trap station

M1, **(b)** upper trap station M2 and **(c)** lower trap M2, respectively, **(d)** upper trap station M4 and **(e)**

lower trap station M4, respectively.

1205

Fig. 6 Phytoplankton productivity records for the tropical North Atlantic. Panels **(a)** – **(e)** show the 1,14-diol fluxes (left *y*-axis; black) and the Diol Index (right *y*-axis; grey) for sediment traps. The *y*-axes are the same for these panels. Wind speed and precipitation data were adapted from Guerreiro et al. (in revision); for references regarding remote sensing parameters, see Guerreiro et al. (2017). Panels **(f)** and **(g)** show the C_{37} alkenone fluxes (left *y*-axis; black) and combined fluxes of *E. huxleyi* and *G. oceanica* (from Guerreiro et al., 2017; right *y*-axis; grey) for the upper traps of M2 and M4.

Fig. 7 (a) Annual mean temperature profiles at the sediment trap locations (World Ocean Atlas 2013) with approximate proxy-lipid production depths indicated, as deduced from Balzano et al. (unpublished results). **(b)** Flux-weighted average (annual) proxy results for the sediment traps compared with the underlying sediments (crosses) and annual mean SST (red line; World Ocean Atlas 2013). Panel **(b)**, **(c)** and **(d)** show the LDI, $U^{K'}_{37}$ and TEX$_{86}$ temperature results, respectively. Triangles reflect sediment trap results (red = upper/~1200 m; blue = lower/~3500 m), and crosses represent surface sediments. In case of the $U^{K'}_{37}$ and TEX$_{86}$, the green and purple triangles and grey crosses reflect the temperatures calculated using the BAYSPLINE and BAYSPAR models (Tierney and Tingley, 2014; 2015; 2018), whereas the other temperatures were calculated by means of the Müller et al. (1998) and Kim et al. (2010; TEX$^H_{86}$) calibrations, respectively. The blue line and crosses in panel **(d)** reflect the depth-integrated temperature for the upper 0-150 m, and subsurface TEX$^H_{86}$ temperatures (Kim et al., 2012). Panel **(e)** shows the flux-weighted average Diol Index values for the sediment traps, and the Diol Index estimates for the surface sediments.
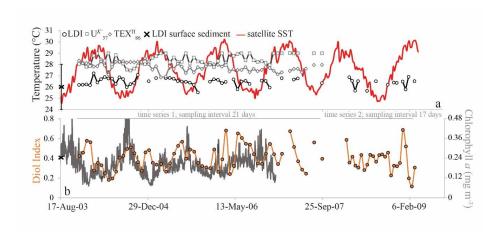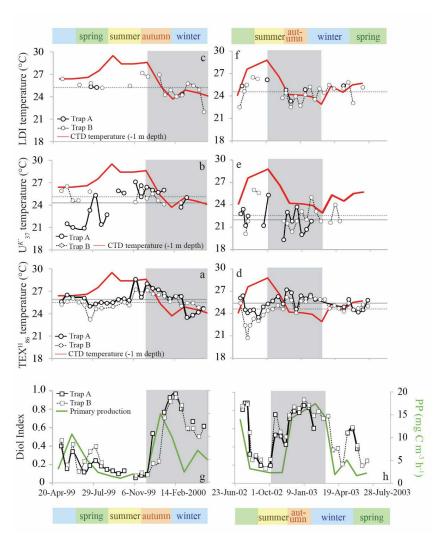
Fig. 8 The LDI-derived temperatures, together with the TEX^H_{86} and $U^{K'}_{37}$-derived temperatures and satellite SST (Fallet et al., 2011) (**a**) and the Diol Index (**b**) for the Mozambique Channel sediment trap. The black cross in panel (**a**) reflects the average LDI temperature of two underlying surface sediments, with the LDI calibration error. The chlorophyll *a* data is from Fallet et al. (2011).

Fig. 9 Seasonal proxy derived temperature and upwelling/productivity records for the sediment traps in the Cariaco Basin. Panels **(a)**, **(b)** and **(c)** show the May 1999 – May 2000 time series TEX^H_{86}-, $U^{K'}_{37}$- and LDI-derived temperature reconstructions for Trap A (275 m depth; solid symbols) and Trap B (455 m depth; dashed symbols), respectively. Panels **(d)**, **(e)** and **(f)** show the proxy data for the July 2002 – July 2003 time series, with CTD-temperatures (1 m depth) in red. The $U^{K'}_{37}$, TEX^H_{86} and CTD temperatures are adopted from Turich et al. (2013). The horizontal lines reflect the average proxy-derived temperatures (Trap A = solid; Trap B = dashed). Panel **(g)** and **(h)** show the 1,14-diol based Diol Index (Rampen et al., 2008) for the 1999-2000 and 2002-2003 time series, respectively, for Trap A (275 m depth; solid symbols) and Trap B (455 m depth; dashed symbols). Primary productivity in mg C m^{-3} h^{-1} is plotted in green (data adopted from Turich et al., 2013). The shaded area reflects the period of upwelling.
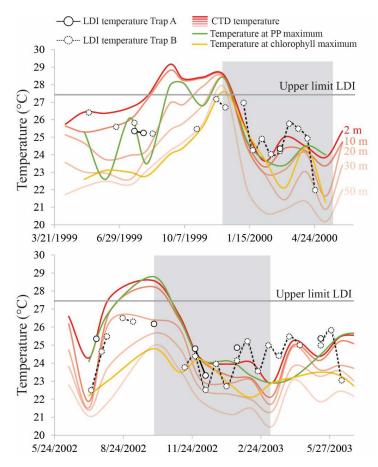
51

1243

Fig. 10 LDI temperature records for the Cariaco Basin time series May 1991 – May 2000 and July 2002
– July 2003 for Trap A (275 m depth; solid symbols) and Trap B (455 m depth; dashed symbols), with
CTD-derived temperatures at 2, 10, 20, 30 and 50 m depth (in red;
http://www.imars.usf.edu/CAR/index.html; CARIACO time series composite CTD profiles), the
temperature at the depth of maximum primary production (green) and the temperature at the depth of
the chlorophyll maximum (yellow; data adapted from Turich et al., 2013). The shaded area represents
the upwelling season.

1251